

Advances in acoustic techniques for evaluating defects and properties in lithium-ion batteries: A review



Yaxun Gou ^{a,b,1}, Yitian Yan ^{a,b,1}, Yan Lyu ^c, Shili Chen ^a, Jian Li ^a, Yang Liu ^{a,b,*}

^a State Key Laboratory of Precision Measuring Technology and Instruments, Tianjin University, Tianjin 300072, China

^b International Institute for Innovative Design and Intelligent Manufacturing of Tianjin University in Zhejiang, Shaoxing 330100, China

^c College of Mechanical Engineering and Applied Electronics Technology, Beijing University of Technology, Beijing 100124, China

ARTICLE INFO

Keywords:

Ultrasound-based detection
LiBs defects
Bulk waves
Guided waves
State of charge
State of health

ABSTRACT

With the rapid demand for high-performance energy storage systems, lithium-ion batteries (LiBs) have emerged as the predominant technology in various applications. However, ensuring the safety and reliability of these batteries remains a critical challenge. Ultrasound-based detection, as a non-destructive and effective method for monitoring the internal state of LiBs, has gradually emerged as a valuable tool to enhance battery safety, reliability, and performance. This paper provides a review of recent advancements in the field of acoustic detection for LiBs, delving into the fundamental principles and mechanisms governing the propagation of acoustic signals within these batteries. This paper reviews the correlation between these acoustic signals and the operational status of the battery, as well as the association with internal side reactions during abnormal conditions. The strengths and limitations of current ultrasound-based detection methods are emphasized, offering insights to guide researchers, engineers, and industry professionals in advancing the field. The review aims to foster the development of robust ultrasound-based detection solutions for the next generation of energy storage systems.

1. Introduction

Based on practical validation, rechargeable batteries built upon clean and environmentally friendly materials are recognized as the most successful and viable energy storage technology to meet energy demands [1,2]. Since their initial introduction in the 1990 s, LiBs have consistently dominated the commercial battery market [1,3,4]. Due to its similarity to composite material structures, LIBs are commonly regarded as a porous, layered structure consisting of an anode, cathode, separator, electrolyte, and a terminal-equipped outer casing [3,5]. LiBs undergo a cyclic process where lithium ions move from the negative electrode(anode) to the positive electrode(cathode) during discharge and return from the positive to the negative electrode during charging. This cyclic behavior of lithium ions ensures the long-term usability of lithium batteries [6,7]. With advantages such as high energy density, lightweight design, extended cycle life, high voltage platform, absence of memory effect, and low self-discharge rate, LiBs have found wide applications in portable electronic devices, electric vehicles, aerospace, and solar energy storage system, among various other fields [8–10].

Presently, the manufacturing process of LiBs remains complex,

involving multiple stages such as slurry blending, coating, drying, calendaring, cutting, vacuum drying, battery assembly, electrolyte injection, formation and aging [11–13]. Simultaneously, there are unknown connections among process parameters, intermediate product performance, and quality characteristics, leading to a high rate of defective products in battery production [14–16]. Consequently, a significant amount of effort is required in the production process for quality control to ensure the efficiency and safety of battery production [17,18].

Safety concerns significantly constrain the broader applications and market expansion of LIBs [19,20]. Apart from potential safety hazards during production, the high energy density of lithium-ion batteries poses a series of safety concerns during general operation process. Moreover, electrical abuse, thermal abuse, and mechanical abuse undoubtedly exacerbate the safety risks associated with lithium batteries in complex environments [21–25]. These forms of abuse can trigger intense side reactions within the battery, leading to rapid degradation and a high likelihood of thermal runaway, resulting in severe safety incidents such as combustion, explosions, and other critical accidents [26,27].

The demand for LIBs has currently reached an unmatched size, with the production capacity expected to experience significant growth in the

* Corresponding author.

E-mail address: ultrasonicslab@tju.edu.cn (Y. Liu).

¹ These authors contributed to the work equally and should be regarded as co-first authors.

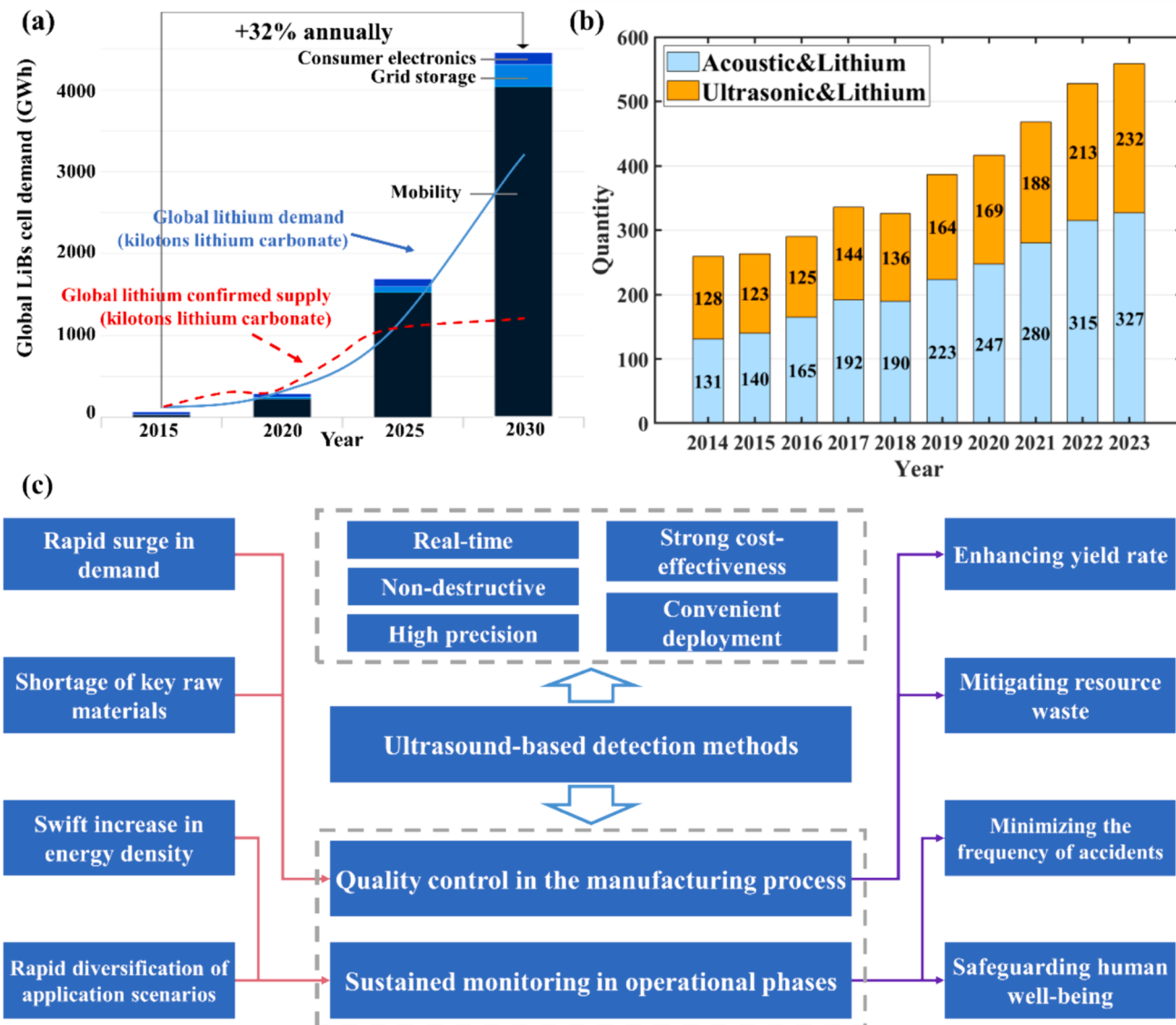


Fig. 1. (a) The global demand variations for LiBs (depicted in a bar chart), along with lithium raw material demand and supply dynamics (illustrated in line graphs) [39,40]. (b) The variation in the publication output of literature on acoustic detection methods and ultrasound-based detection methods for LiBs over the past decade, statistical data sourced from Web of Science. (c) Demand, applications, characteristics, and significance of ultrasound-based detection methods for LiBs.

coming years (see Fig. 1a) [8–11]. Therefore, there is an urgent need for real-time, convenient, and non-destructive detection technologies to precisely monitor the battery state and reduce potential hazards. This demand has led to the development of various advanced characterization techniques [28–30], such as electrochemical impedance spectroscopy [31,32], transmission electron microscopy [33], neutron imaging [34,35], nuclear magnetic resonance [36], and X-ray computed tomography [37]. The equipment required for these techniques typically involves a significant amount of laboratory tools, space, and funding, thus presenting high barriers to widespread adoption and application [38].

In the past decade, ultrasound-based detection methods, including acoustic emission (AE) and ultrasonic testing (UT), have increasingly been employed for non-destructive, real-time diagnostics of LiBs, providing a fresh perspective on battery performance and safety [14,41]. At the same time, research articles on acoustics and ultrasonic detection of lithium-ion batteries are rapidly increasing (see Fig. 1b). AE technology is a passive monitoring tool capable of detecting acoustic events occurring within materials or devices [42]. When materials or devices undergo stress, resulting in deformation or even cracking,

spontaneous acoustic emission events occur. Unlike traditional forms of stress, acoustic emission events in lithium batteries are typically determined by internal physical and chemical changes, such as electrode cracking, gas evolution, electrode deformation, and SEI formation [43–47]. AE technology is highly sensitive to the formation and progression of minor damage, making it commonly used for detecting micro-damage in batteries [48–50]. UT is an active technique involving the introduction of externally generated acoustic signals and their propagation through a material to study internal structures and processes [51,52]. As ultrasonic waves propagate through the battery, reflecting and transmitting multiple times at interfaces due to differences in acoustic impedance between material layers, the attenuation and shift of acoustic signals can effectively correlate with the evolving processes within the battery [53–57]. Additionally, the scanned ultrasonic signals, through further data processing, can yield visual results such as 2D/3D images [58,59]. Currently, ultrasound-based methods have achieved significant success in lithium-ion battery diagnostics. We believe that the integration of cost-effective, non-destructive ultrasonic testing methods with the increasingly diversified market demand for lithium-ion batteries will play a crucial role in safeguarding human

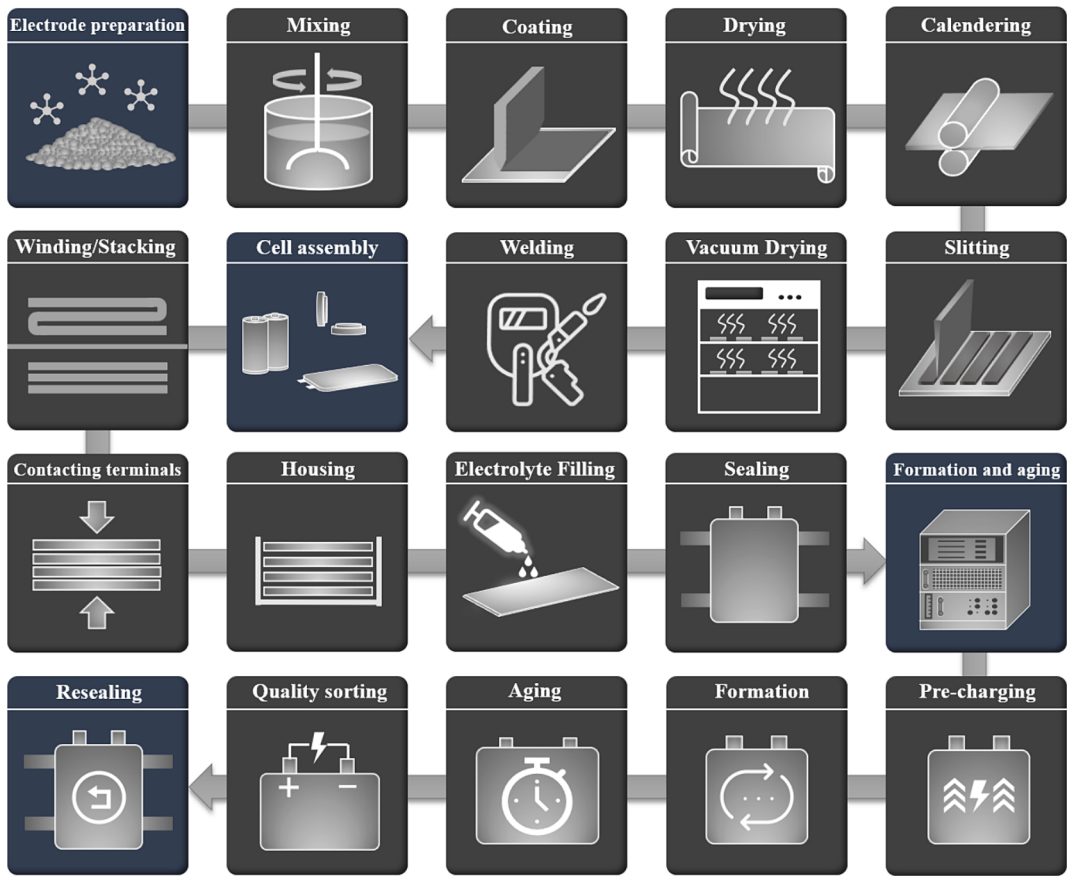


Fig. 2. Schematic of LiBs manufacturing processes. The deep blue blocks represent the four primary stages of the manufacturing process, followed by the gray blocks, which depict key manufacturing processes within each stage. (For interpretation of the references to color in this figure legend, the reader is referred to the web version of this article.)

health and welfare, as well as reducing resource wastage (see Fig. 1c).

In this review, we systematically present acoustics-based detection methods applied to internal state monitoring of LiBs. Combining principles with practical application cases, we discuss the advantages and disadvantages of existing technologies and provide insights into future directions. The structure of this paper is as follows: In Sections 2, we highlight the urgent need for real-time and convenient in-situ detection technologies in the manufacturing and usage processes of LiBs. In Section 3, we primarily introduce the principles of ultrasound-based detection methods for battery diagnostics. In Section 4, we systematically discuss and summarize the latest advancements in ultrasound-based state evaluation for LiBs, along with the challenges and potential impacts of these new technologies. In Section 5, perspectives on future developments in ultrasound-based LiBs evaluation technologies are presented. Finally, in Section 6, we provide a summary of the entire paper. We hope that this paper contributes to fostering more collaboration between the academic and industrial sectors, further leveraging ultrasound-based detection technologies to advance the development of LiBs technology.

2. Critical ultrasound-based detection requirements for LiBs

The longevity, performance, and safety of LiBs face threats from imperfect manufacturing processes and operation. This section concentrates on key manufacturing processes, general operation and prevalent abuse scenarios, addressing challenges in quality control during manufacturing and ensuring operational safety. Special emphasis is placed on the vital role of in-situ ultrasound-based detection methods in enhancing battery manufacturing techniques and formulating effective battery management strategies.

2.1. Quality control in the manufacturing process

After years of development, the production of lithium batteries has reached a mature stage, involving key steps as shown in Fig. 2, which includes four major steps: electrode preparation, cell assembly, formation, and aging, encompassing nearly 20 sub-steps [11,12,18]. The formation process (where the cell undergoes repeated charging and discharging cycles, leading to the formation of a stable Solid Electrolyte Interphase (SEI) layer on the anode) and the aging process (where the cell is placed on aging racks to facilitate complete electrolyte wetting and stabilization of the SEI layer) also require several weeks to complete [60,61]. The complexity of the production process can result in various defects. Uneven electrode materials, contamination, insufficient drying, and cracking can lead to inconsistent electrochemical performance in different areas and uneven degradation of active electrode materials, resulting in localized heat accumulation within the battery [57,58]. Inadequate electrode wetting can restrict electrochemical reactions in certain areas of the cell, thereby reducing overall battery performance [62,63]. Poor SEI development can impede ion transfer between the electrode active material and the electrolyte or insufficiently isolate them, thus decreasing overall battery performance, increasing side reactions, and potentially causing severe safety issues. Currently, ultrasonic inspection cannot directly monitor SEI growth and abnormalities. The sensitivity of acoustic signals to the properties of the medium and gas interfaces helps to observe dynamic changes in real-time without damaging the battery structure. Analyzing acoustic wave parameters can provide in-situ observation of electrode preparation, assembly, and formation, offering strong support for assessing battery manufacturing quality.

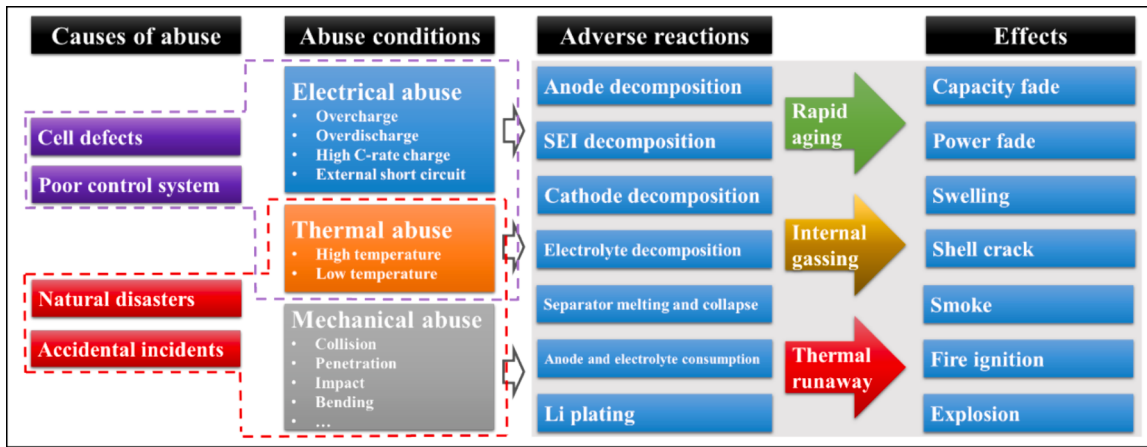


Fig. 3. Overview of LiBs abuse issues.

2.2. State monitoring in general operation

Under general operating conditions, it is necessary monitor the state of charge (SOC) and state of health (SOH) of lithium-ion batteries to manage their usage and retire batteries that reach specific low-capacity limits [64]. During battery charging, the low potential difference between the electrode and electrolyte at the anode induces side reactions, consuming electrolyte and recoverable Li^+ ions, forming a solid electrolyte interphase (SEI) on the anode particles, and generating gases such as CH_2 , C_2H_4 , H_2 , and CO [65,66]. This results in the loss of active material and a decrease in conductivity. These side reactions are considered the main causes of capacity and power degradation [67]. Additionally, the solid-state diffusion of lithium ions into and out of the electrode particles during charging and discharging causes diffusion-induced stress (DIS) and volume changes within the electrode particles. These stresses can have various effects on the electrode, such as mechanical fatigue and fracture of electrode particles, isolation of electrode particles from the composite matrix, or SEI fracture [68]. Changes in material properties during the charge–discharge cycle can be correlated with certain characteristics of ultrasonic signals [69–72], and are sufficiently sensitive to identify defects within the electrodes [56]. Moreover, ultrasonic methods can effectively capture acoustic impedance mismatches caused by gas evolution during side reactions [59,73]. Considering the convenience, flexibility, and low spatial footprint of deploying ultrasonic sensing systems, using ultrasonic methods for real-time monitoring of battery conditions under general operating conditions holds significant potential and application prospects.

2.3. Safety assessment of LiBs abuse

Conventionally, materials with high energy density tend to manifest lower thermal stability and heightened safety risks [22,74]. The safety performance of LiBs is subject to diverse factors, particularly under abuse conditions [75,76]. Fig. 3 illustrates the categorization of abuse conditions into three types: electrical, thermal, and mechanical, accompanied by a listing of their common causes, resulting adverse reactions, and impacts on LiBs [76,77].

2.3.1. Electrical abuse

Due to the inherent non-uniformity of batteries, electrical abuse occurs during conditions of overcharging, over-discharging, high-rate charging, or external short circuits, resulting in a series of adverse electrochemical reactions [20].

Overcharging typically occurs when a battery is forcefully charged beyond its cutoff voltage or exceeds its designated capacity level. Overcharging leads to excessive de-lithiation of the cathode layered oxide, structural breakdown, decomposition of active materials, severe

side reactions, and the release of oxygen, among other issues [78]. The continuous deposition of lithium dendrites may penetrate the separator, causing internal short circuits that can result in thermal runaway and serious safety incidents, such as rupture, combustion, and explosion [79,80].

Over-discharging refers to discharging a battery below the lower limit set by the electrochemical electrode coupling [81]. In comparison to overcharging, over-discharging is relatively safer as it is less possible to induce thermal runaway [82]. In the reductive process following deep discharge, the anode may form copper dendrites [82–84]. Simultaneously, excessive de-lithiation may decompose the SEI layer, releasing heat and generating gases such as carbon dioxide and methane [85]. These phenomena may result in a significant temperature elevation, expansion, and intensify thermal risks [85–87].

Frequent high-speed charging may impact the power, energy, safety, and lifespan of LiBs [88]. Charging at excessively high C-rates can lead to phenomena such as polarization and lithium deposition [89–92]. Additionally, excessive lithium imbalance may affect the mechanical integrity of the battery, leading to degradation of electrode materials, including layer cracking, fissures, and electrode isolation [93–95].

External short circuits can cause the uniform and rapid release of heat from the battery [96]. Internally, the diffusion of lithium ions in the negative electrode restricts the current rate, while the heat generated from side reactions, such as electrolyte decomposition in the positive electrode, may still cause a rapid temperature rise. This can lead to expansion, rupture, gas release, and even trigger thermal runaway, posing safety risks [45,96,97].

2.3.2. Thermal abuse

LiBs involve a risk of thermal abuse under extreme temperatures [98,99]. Research indicates that temperatures exceeding 60 °C trigger the decomposition and regeneration of the SEI. The exposed lithiated anode material rapidly reacts with the electrolyte, causing a swift decline in battery capacity and generating significant amounts of gas and heat [100]. This external thermal decomposition and regeneration of the SEI persist until a highly exothermic decomposition of the graphite phase occurs at approximately 220 °C [101]. Rapid external thermal reactions involving the electrolyte, lithiated graphite, and lithiated graphite anode material take place within the temperature range of 200–260 °C [101]. Without intervention, this process continues until reactants are depleted, ultimately resulting in severe failure of commercial batteries, including fires and explosions, accompanied by the release of flammable and toxic gases [102,103].

In addition to high-temperature environments, LiBs also exhibit performance degradation in extremely low-temperature conditions [104,105]. At low temperatures, the viscosity of the electrolyte increases, reducing the conductivity of lithium-ion [5,6]. This decelerates

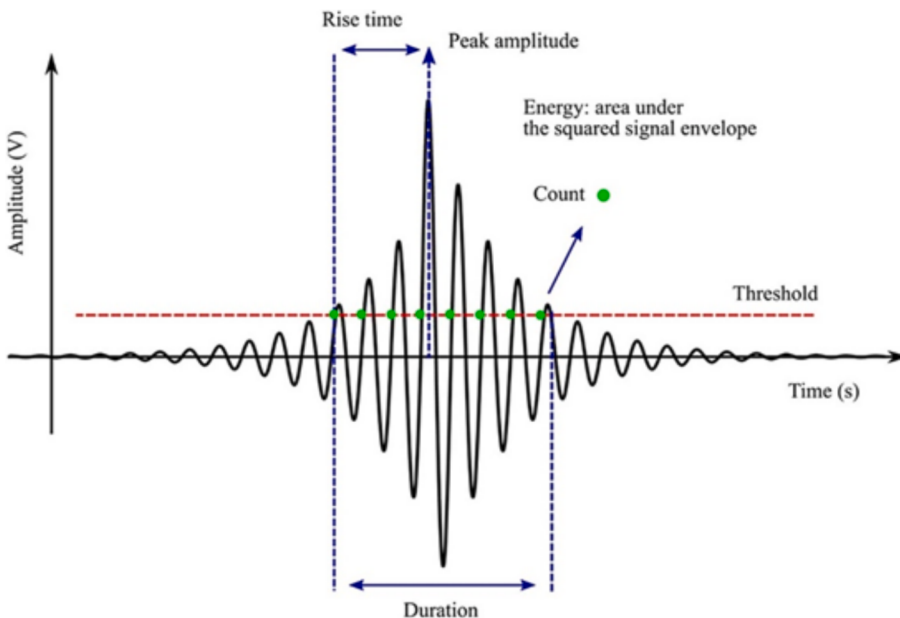


Fig. 4. A typical AE time-domain waveform and its main acoustic features [14].

the kinetics of electrochemical reactions [106,107]. Additionally, low temperatures hinder charge transfer at the electrode/electrolyte interface and the transport of lithium-ion within the SEI, electrolyte, and electrode, resulting in performance degradation [105]. Low temperatures also cause a reduction in lithium-ion diffusion in graphite, and the lithiation process is generally slower than the delithiation process at -20°C [108]. During the battery charging process, lithium deposition on the anode surface accelerates, with a significant portion becoming “non-active lithium” that no longer participates in subsequent electrode reactions. This is a primary factor contributing to capacity decay [109,110].

2.3.3. Mechanical abuse

External mechanical loads have the potential to inflict damage on batteries through deformation and foreign object penetration, resulting in internal short circuits and thermal runaway. This, in turn, can lead to battery damage or safety incidents [111,112]. In summary, mechanical abuse loads, encompassing compression [113], indentation [114], bending [115], and penetration [116], may yield six possible outcomes for batteries: (a) deformation without internal short circuit, (b) deformation with material fracture but no internal short circuit, (c) deformation with material fracture, internal short circuit, voltage recovery, and no subsequent internal short circuit, (d) deformation with material fracture, internal short circuit, and battery venting, (e) deformation with material fracture, internal short circuit, significant thermal runaway, and (f) deformation with material fracture, internal short circuit, thermal runaway, and explosion [112,117].

In conclusion, LiBs may undergo internal structural damage and material transformations during various instances of abuse, leading to performance degradation and posing potential risks of thermal runaway, smoke generation, combustion, or even explosion. Consequently, there is an urgent need for real-time, rapid, user-friendly, and cost-effective in-situ detection and mechanistic analysis of LiBs abuse. Ultrasound-based detection methods can meet these requirements, effectively characterizing the secondary reactions associated with various battery abuse scenarios, including but not limited to electrode material cracking and degradation, internal gas generation, electrolyte leakage and decomposition, transition metal dissolution, and lithium deposition with dendrite formation. Furthermore, integrating ultrasound-based methods with temperature monitoring, thickness measurement, and other techniques enables accurate identification of the type of battery misuse,

providing crucial insights for developing effective battery management, ensuring safety, and guiding future development strategies.

3. Ultrasound-based detection principles of LiBs

The earlier sections explored the complexities of LiBs manufacturing and potential abuse scenarios. Given the intricate manufacturing processes and diverse applications, there is a critical demand for in-situ, real-time, and precise monitoring of LiBs operations and internal conditions. Ultrasound-based detection techniques emerge as a promising solution, offering notable cost-effectiveness and deployment ease. The subsequent section offers a concise theoretical overview of AE and UT techniques in battery diagnostics.

3.1. Acoustic emission

In battery diagnostics, AE enables precise identification of internal changes, including gas evolution, electrode deformation, and crack development. The analysis of acoustic emission signals is primarily categorized into time-domain and frequency-domain analyses. Typical acoustic emission signals and common signal features are illustrated in Fig. 4 [14,118]. Time-domain acoustic emission signals have several critical features. Firstly, setting a waveform amplitude threshold is a common method to eliminate background noise and enhance the signal-to-noise ratio.

Signal amplitude (SA) is a vital feature in acoustic diagnostics, reflecting the detectability of acoustic emission events. It is typically expressed in decibels as shown in Eq. (1), where A is the amplitude, V_{sig} is the measured signal voltage, and V_{ref} is the reference voltage.

$$A = 20 \log \frac{V_{\text{sig}}}{V_{\text{ref}}} \quad (1)$$

Besides amplitude, parameters such as rise time (the interval from the first threshold crossing to the peak amplitude), signal energy, and duration (the time between the first and last threshold crossings) are crucial.

Frequency-domain analysis offers a wider range of features for acoustic emission signal analysis. Techniques like Discrete Fourier Transform (DFT) convert signals from the time domain to the frequency domain and effectively extract the amplitude spectrum. Key frequency-

domain features such as peak frequency, centroid frequency, and spectral kurtosis are crucial for identifying AE sources and characterizing defect types [48,119].

Additionally, methods like Short-Time Fourier Transform (STFT) and Wavelet Transform (WT) provide dynamic representations of frequency changes over time. These are helpful for capturing transient events or changes in frequency content of acoustic emission signals, aiding in the analysis of lithium battery cycling aging mechanisms [43].

Analyzing these key parameters together offers a comprehensive description of acoustic emission events in the assessment of the dynamic performance of lithium batteries.

3.2. Ultrasonic detection

3.2.1. Bulk waves

In ultrasonic testing, bulk waves refer to ultrasonic waves within a material [69,70,120]. During battery cycling, electrochemical changes in the intercalation material can alter mechanical performance, impacting measurement parameters like Time of Flight (ToF) and SA. The definition of ToF is given by Eq. (2):

$$ToF = \frac{L}{V_p} \quad (2)$$

where L represents the propagation path of ultrasonic waves within the battery. When employing the transmission method to collect signals, L equals the thickness of the battery. Conversely, when utilizing the reflection method to gather signals, L is equal to twice the thickness of the battery, D represents the thickness of the battery, and V_p represents the longitudinal wave propagation velocity within the battery.

According to equation (2), ToF primarily depends on variations in battery thickness and the speed of sound. In typical LiBs, the expansion of the graphite anode due to lithium ion insertion leads to battery expansion during charging [121]. Additionally, Koyama et al. [122] observed expansion in the LCO cathode during lithium deintercalation. Although an increase in battery thickness usually results in increased ToF, multiple experiments indicate a decrease in ToF during charging [69,123]. This highlights a more pronounced impact of internal material property changes on the speed of sound and underscores the limitations of assessment methods solely based on thickness measurements. Currently, a series of battery models, including the composite homogenization model, Biot's model, and slurry models [124–127], has been developed to solve for the internal speed of sound in batteries.

The composite homogenization model treats the electrode model as an isotropic medium, assuming uniform behavior and characteristics in all directions. This simplifies the model establishment and analysis process. For isotropic elastic materials, the wave propagation velocity can be described by Eqs. (3)–(5) [70,128]:

$$V_p = \sqrt{\frac{K + \frac{4}{3}G}{\rho}} \quad (3)$$

$$K = \frac{E}{3(1 - 2\nu)} \quad (4)$$

$$G = \frac{E}{2(1 + \nu)} \quad (5)$$

where E refers to the LiBs's Young's modulus, K and G respectively denote the bulk modulus and shear modulus of the LiBs's, and ρ and ν respectively represent the density and Poisson's ratio of the LiBs's.

Throughout battery charge–discharge cycles, both battery parameters [129] and the elastic modulus [130] experience linear changes, influencing wave velocity and subsequently impacting wave propagation time within the battery [128]. However, the battery interior is typically not perfectly isotropic, limiting the effectiveness of the composite homogenization model. This effect results in the experimental

first arrival time consistently being slower than the expectation [70,131].

To address the limitations of the composite homogenization model, the Biot's model is introduced for describing ultrasonic wave propagation in fluid-saturated porous media [125,127]. Biot's model demonstrated the existence of three waves in the absence of dissipative forces: one shear wave and two compressional waves [132]. Typically, researchers tend to focus on studying the variation of longitudinal wave velocities with charging cycles.

Biot demonstrated that when the experimental frequency is more than one order of magnitude below the critical frequency f_t (see Eq. (6)), the relative deviation between the fast wave velocity V_p and the reference wave velocity V_c in porous media is approximately 10^{-4} . Therefore, it can be assumed that they are equal (refer to Eq. (7)) [133].

$$f_t = \frac{\pi\mu}{4\rho_L d^2} \quad (6)$$

where μ represents dynamic viscosity, ρ_L represents density, and d represents the pore size of the porous medium.

Based on Biot's low-frequency approximation and a series of assumptions, the fast wave velocity V_p , slow wave velocity V_L , and shear wave velocity V_s can be determined from Eqs. (7)–(10) [125,127]:

$$V_p \cong V_c = \sqrt{H/\rho} \quad (7)$$

$$\rho = (1 - \nu)\rho_S + \nu\rho_L \quad (8)$$

$$V_L = V_c \sqrt{2 \frac{f}{f_c} \frac{\sigma_{11}\sigma_{22} - \sigma_{12}^2}{\gamma_{12} + \gamma_{22}}} \quad (9)$$

$$V_s = \sqrt{\frac{N_n}{\rho_{11}(1 - \frac{\rho_{12}^2}{\rho_{11}\rho_{12}})}} \quad (10)$$

where H represents the Biot's coefficient, determined by the elastic modulus of the solid and liquid phases of the electrode, along with porosity, ρ is the average density of the porous medium in the lithium-ion battery, ν denotes the porosity of the battery, σ is a parameter defining elastic properties, γ is the dynamic property parameter, f_c is the characteristic frequency, and N_n is the shear modulus of the drained porous matrix.

The Biot's model, with more variable parameters than the composite homogenization model, aligns closely with the battery's characteristics. However, experimental observations show differences between predicted sound velocity and actual results. Gold et al. [134] suggested that experiments may capture the shear wave in the Biot's model, without explaining the absence of the more easily collected longitudinal waves [135]. Huang et al. [136] argued that using the Biot's model for the entire battery may lack fundamental accuracy. As a solution, Huang proposed employing the slurry model for the electrode and the Biot's model for the separator [137]. Observationally, collected wave packets likely represent the longitudinal wave, indicating that wave velocity inside the battery is closer to the liquid electrolyte than the porous solid. The estimated longitudinal wave velocity based on the slurry model is as follows [126,136]:

$$V_p = \sqrt{\frac{K}{\rho}} \quad (11)$$

$$\frac{1}{K} = \frac{\nu}{K_S} + \frac{1 - \nu}{K_L} \quad (12)$$

$$\rho = \nu\rho_S + (1 - \nu)\rho_L \quad (13)$$

where S and L refer to the solid phase and liquid phase of the slurry, respectively, and ν is the volume fraction of the solid phase. K is the

comprehensive volume modulus of the solid and liquid phases [126]. ν needs to be calculated in advance, commonly using the mercury porosity determination method [138,139].

Incorporating material properties into the model enables the determination of the actual bulk modulus and density of the battery, thereby deriving the corresponding wave velocities. This enables precise calculations of ToF.

The SA is another crucial characteristic in analyzing ultrasonic signals, with variations primarily dependent on changes in battery thickness leading to alterations in acoustic attenuation rates and transmission coefficients. However, the anisotropy nature, porosity, viscoelasticity, and other characteristics of battery materials pose challenges in the analysis of signal attenuation [140].

Amplitude is typically considered a characteristic of acoustic energy, directly correlated with the energy attenuation of bottom echoes. In a single material, the definition of SA is given by Eq. (14) [141]:

$$A_x = A_0 \times \exp(-\alpha_i x) \quad (14)$$

where A_x represents the SA at a distance x from the ultrasonic source, and α_i is the attenuation rate of ultrasonic waves in the material i .

Many researchers posit that, during the charge–discharge cycling of batteries, material damping undergoes changes, altering the attenuation rate of ultrasound and consequently leading to variations in SA [128,142].

Besides acoustic attenuation, the magnitude of SA is also determined by the impedance differences at interfaces between different materials. According to numerous scholars, ultrasonic signals exhibit scattering when propagating through layered materials in batteries. The definitions of ultrasonic impedance, transmission and reflection coefficients are as follows [143]:

$$Z_i = \rho_i \times v_i \quad (15)$$

$$T_{ij} = \frac{4Z_i Z_j}{(Z_i + Z_j)^2} \quad (16)$$

$$R_{ij} = 1 - T_{ij} \quad (17)$$

where ρ_i represents the density of the i th layer material; v_i is the velocity of waves in the material i ; Z_i represents the impedance of ultrasound in materials; T_{ij} is the transmissivity of ultrasound from material i to material j ; R_{ij} is the reflectivity of ultrasound from material i to material j .

In summary, a profound understanding of the mechanisms underlying the variation of ToF and SA throughout the battery cycling process establishes a robust theoretical foundation for analyzing the defect formation and operational states of the battery.

3.2.2. Guided waves

Ultrasonic guided waves (UGW) typically refer to waves that propagate along the surface or interior of a medium [144]. Guided wave detection entails solving the wave equation with specific boundary conditions to obtain the dispersion curve, providing key properties such as phase velocity and wave number. The definition of the ToF for guided wave propagation is as follow:

$$ToF = \frac{L_a}{V_g} \quad (18)$$

where L_a represents the distance between two transducers, and V_g is the group velocity of the guided wave propagation.

Ladpli et al. [72] initially proposed the concept of LiBs as a multi-layered material system. This approach describes the wave propagation by leveraging the specific material properties and geometric characteristics of each layer. The key of this multi-layer model involves formulating the wave equations and applying appropriate boundary conditions to interrelate the displacements and stresses across the layers.

The three-dimensional equation of motion for waves propagating in an infinite medium is given by [128,145]:

$$\rho \frac{\partial^2 \mathbf{u}}{\partial t^2} = (\lambda + \mu) \nabla(\nabla \cdot \mathbf{u}) + \mu \nabla^2 \mathbf{u} \quad (19)$$

where $\mathbf{u}(u_1, u_2, u_3)$ represents the displacement field of the wave, ρ is the material density, and λ and μ are Lamé stiffness constants.

In guided wave inspection of pouch cells (center frequency between 100 and 200 kHz), the guided wave wavelength is significantly smaller than the battery's structural dimensions, validating the plane strain assumption. Consequently, the governing equations for the battery's layers can be simplified to two-dimensional equations [146]. By employing potential function analysis or partial wave analysis to solve the wave equations for each layer, we derive the displacement and stress solutions. Therefore, appropriate boundary conditions at the interfaces couple these solutions into a unified system of motion equations [128,147]. Subsequently, numerical solutions for the dispersion curve can be efficiently obtained using global matrix methods or transfer matrix methods [148,149].

Utilizing the group velocity-to-phase velocity conversion formula provides the group velocity dispersion curve, enabling the determination of the ToF:

$$V_g = d(kV_p)/dk \quad (20)$$

In addition to the multi-layer isotropic modeling of pouch cells, Gao et al. [150,151], based on the characteristics of LiBs and Biot's theory, abstracted the lithium-ion battery as a saturated multi-layer porous structure. The wave motion equation in the porous medium is given by:

$$\sigma_{ij,i}^m = \frac{\partial^2}{\partial t^2} (\rho_{11}^m u_j^m + \rho_{12}^m U_j^m) + b^m \frac{\partial}{\partial t} (u_j^m - U_j^m) \quad (21)$$

$$s_i^m = \frac{\partial^2}{\partial t^2} (\rho_{12}^m u_j^m + \rho_{22}^m U_j^m) - b^m \frac{\partial}{\partial t} (u_j^m - U_j^m) \quad (22)$$

where σ_{ij} is the stress of solid phase; s is the stress of fluid phase; u^m is the solid phase displacement, U^m is the fluid phase displacement; ρ_{11} , ρ_{12} , and ρ_{22} represent the densities of the solid phase, the solid–liquid coupled phase, and the fluid phase, respectively, b^m is the dissipation coefficient.

The constitutive equations for the m -th layer of fluid-saturated porous media based on Biot's theory are given as follows.

$$\sigma_{ij}^m = 2N^m \zeta_{ij}^m + \delta_{ij} (A^m \mathbf{e}^m + Q^m \mathbf{e}^m) \quad (23)$$

$$s^m = Q^m \mathbf{e}^m + R^m \mathbf{e}^m \quad (24)$$

where ζ_{ij}^m is the shear strain of solid phase, \mathbf{e}^m and \mathbf{e}^m respectively denote the solid volume strain and the fluid volume strain, and A^m, N^m, Q^m and R^m are Biot's elastic coefficients.

Then, by substituting Eqs. (23) and (24) into Eqs. (21) and (22), the governing equations can be obtained as follows:

$$\begin{aligned} N^m \nabla^2 \mathbf{u}^m + \text{grad}[(A^m + N^m) \mathbf{e}^m + Q^m \mathbf{e}^m] \\ = \rho_{11}^m \frac{\partial^2 \mathbf{u}^m}{\partial t^2} + \rho_{12}^m \frac{\partial^2 \mathbf{U}^m}{\partial t^2} + b^m \frac{\partial}{\partial t} (\mathbf{u}^m - \mathbf{U}^m) \end{aligned} \quad (25)$$

$$\text{grad}[Q^m \mathbf{e}^m + R^m \mathbf{e}^m] = \rho_{12}^m \frac{\partial^2 \mathbf{u}^m}{\partial t^2} + \rho_{22}^m \frac{\partial^2 \mathbf{U}^m}{\partial t^2} - b^m \frac{\partial}{\partial t} (\mathbf{u}^m - \mathbf{U}^m) \quad (26)$$

When acoustic waves propagate between adjacent layers (fluid-saturated porous media), the continuity boundary conditions that need to be satisfied are:

$$\frac{\partial u_3^m}{\partial t} = (v_3^{d \rightarrow V_m})^+ = (v_3^{d \rightarrow V_{m+1}})^- = \frac{\partial u_3^{m+1}}{\partial t} \quad (27)$$

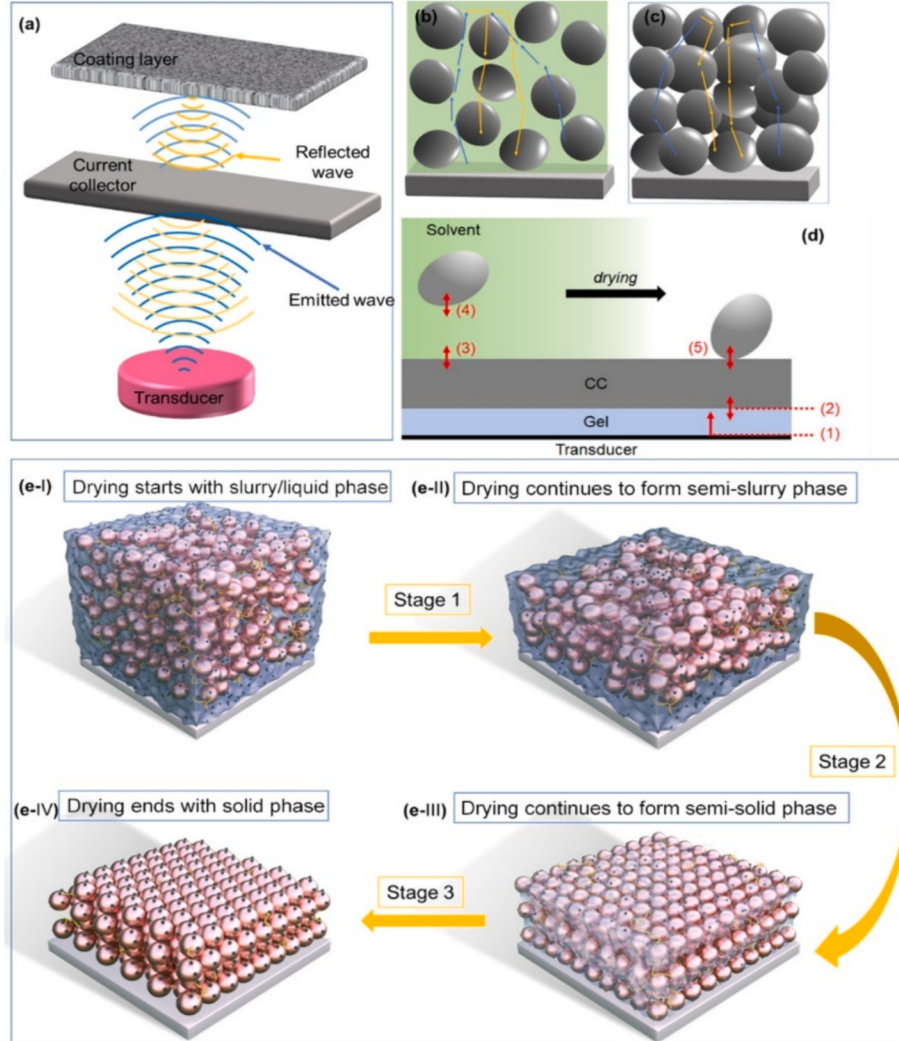


Fig. 5. (a) Schematic diagram of the ultrasonic reflection of the electrode, (b) schematic diagram of reflected paths of ultrasonic waves through a wet slurry electrode coating with solvent, (c) schematic diagram of the reflected paths of the ultrasonic waves through the dried solid electrode, (d) schematic diagram of interfaces in the electrode drying process, in which ToF shifts occur as interface (3–4) diminishes and transits to interface (5), (e) three-stage drying mechanism: stage 1 is from the slurry phase (e-I) to form a semi-slurry (e-II), stage 2 follows with further removal of the solvent (e-III), and stage 2 ends with a compacted solid film of coating (e-IV) [57].

$$\frac{\partial u_1^m}{\partial t} = (v_1^{d \rightarrow V_m})^+ = (v_1^{d \rightarrow V_{m+1}})^- = \frac{\partial u_1^{m+1}}{\partial t} \quad (28)$$

$$n^m(v_3^{f \rightarrow V_m} - v_3^{d \rightarrow V_m})^+ = n^{m+1}(v_3^{f \rightarrow V_{m+1}} - v_3^{d \rightarrow V_{m+1}})^- \quad (29)$$

$$(\sigma_{33}^{s \rightarrow M_1})^+ + (\sigma_{33}^{f \rightarrow M_1})^+ = (\sigma_{33}^{s \rightarrow M_2})^- + (\sigma_{33}^{f \rightarrow M_2})^- \quad (30)$$

$$(\sigma_{13}^{d \rightarrow V_m})^+ = (\sigma_{13}^{d \rightarrow V_{m+1}})^- \quad (31)$$

$$\frac{(\sigma_{33}^{f \rightarrow V_m})^+}{n^m} = \frac{(\sigma_{33}^{f \rightarrow V_{m+1}})^-}{n^{m+1}} \quad (32)$$

In this context, V_m represents the LiBs of the m^{th} layer, n denotes the porosity, and upper and lower interfaces are denoted by “+” and “−”. Additionally, d represents the solid component, f is the liquid component, and σ signifies the stress component.

Currently, although some research has been conducted on dispersion curve models for pouch and cylindrical cells, further in-depth studies are needed to enhance simulation effectiveness and model generality [150,152].

4. Applications of ultrasound-based detection on LiBs

Ultrasound-based methods find extensive applications in the fields of battery detection and state assessment. This section explores the applications of ultrasound-based detection in areas such as electrode defects, internal gas generation, capacity assessment, and aging state evaluation.

4.1. Electrodes

The electrode plays a crucial role in LiBs. Non-uniformities in electrode materials arising from the manufacturing process, along with mechanical defects and damage due to abuse conditions, pose direct threats to the lifespan and safety of LiBs.

Several studies have attempted to use AE technology to assess in-situ damage in electrode materials. The feasibility has been demonstrated on graphite-based [153], Si [154], manganese oxide [45], LCO [44], S [155], and $\text{Co}_{0.2}\text{Cu}_{0.2}\text{Mg}_{0.2}\text{Ni}_{0.2}\text{Zn}_{0.2}\text{O}$ [156] electrode batteries. Ohzuku et al. [50] pioneered the use of AE technology to detect cracks in manganese dioxide cathodes. They found that particle fractures correlate positively with discharge current during lithium-ion insertion into the solid electrode matrix. Choe et al. [46] detected explosive and

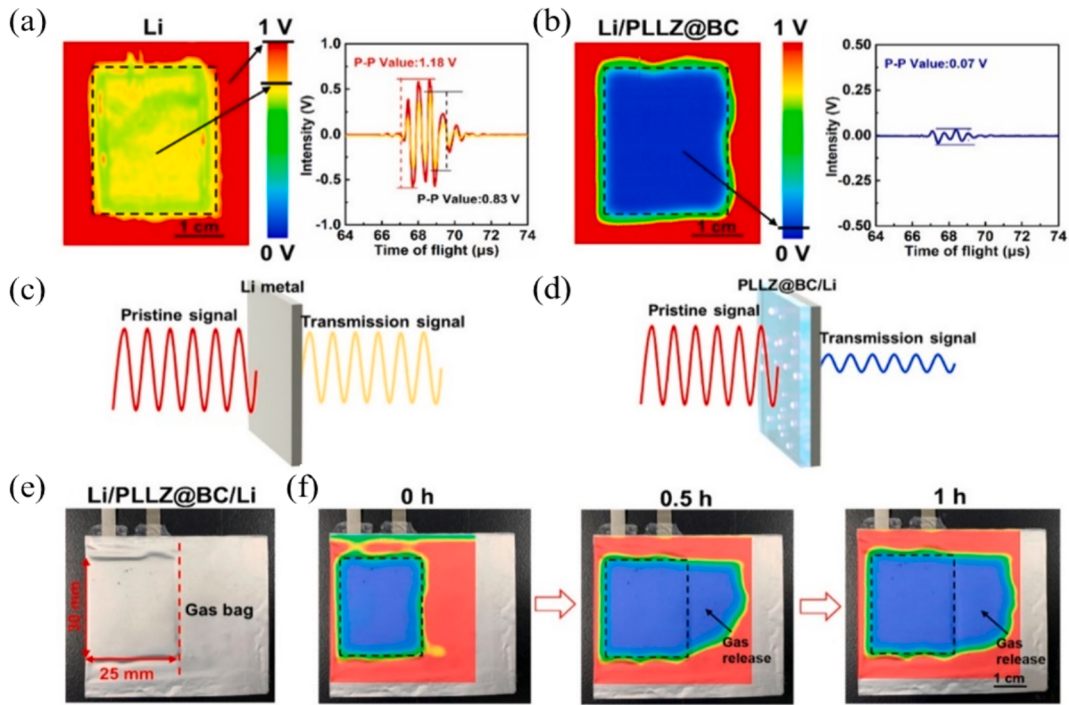


Fig. 6. Gas detection in a lithium/PLLZ@BC/lithium pouch cell. (a) Ultrasound transmission image of lithium metal and ultrasound waves marked by arrows, (b) Ultrasound transmission image of PLLZ@BC/lithium and ultrasound waves marked by arrows. Ultrasound signals passing through (c) lithium metal and (d) PLLZ@BC/lithium schematic diagrams. (e, f) Photographs of Li/PLLZ@BC/lithium pouch cell and corresponding overlaid ultrasound transmission images after 0 h (no rest after assembly), 0.5 h, and 1 h of storage [73].

continuous AE signals released during particle cracking and SEI layer formation in LCO/graphite full-cell LIBs. They independently assessed the damage to each electrode by combining the cumulative AE hit counts for each waveform. Etiemble et al. [157] investigated the fragmentation of LaNi₅-based electrodes with different Co contents through AE measurements, demonstrating that electrode fractures primarily occur during the first charging cycle. Didier-Laurent et al. [48] identified two distinct AE signals during the charge/discharge cycles of MH alloy electrodes, characterized by high energy and short rise time, and low energy and long rise time, attributing the former to electrode particle fractures. Tranchot et al. [49] identified AE signals intensified by electrode fractures during the initial lithiation of silicon-based electrodes, caused by the formation of the c-Li₁₅Si₁₄ phase. Similar findings were reported by Rhodes et al. [154] and Kalnaušas et al. [158] in silicon-based electrode studies, with noticeable AE emission bursts during subsequent charge and discharge steps.

AE signals can be significantly correlated with electrode fracturing during the first charge–discharge cycle, predominantly capturing electrode fracturing occurring primarily during the initial charge–discharge cycle. This technique enables continuous and real-time monitoring of electrode fracturing during battery manufacturing. However, current efforts only allow for qualitative detection, lacking precise quantitative characterization. Further research is expected to establish quantitative correlations between the intensity of AE signals and the number of impacts as well as the extent of electrode fracturing.

In addition to AE technology, UT has also been applied to LiBs electrodes. Robinson et al. [56] conducted pulse-echo spectrum analysis on batteries with artificially embedded defects, achieving the localization of defects at the micrometer scale in cathode deposition. Zhang et al. [57] utilized the dynamic evolution of ultrasonic reflection signals' attenuation and ToF correlation in NMC622 cathodes and graphite anodes during drying process, associating it with a three-stage drying mechanism. They achieved real-time changes in ultrasonic signals at different drying stages and recorded the duration of each stage for batteries of different thicknesses, as illustrated in the Fig. 5. Bauermann

et al. [54] used scanning acoustic microscopy (SAM) with a resolution of 40 μm/pixel to visualize defects in button cells and pouch cells, including coating non-uniformities, cracks and wrinkles on electrodes [55]. Yi et al. [58] utilized tomographic scanning to detect and locate metal contaminants on the electrode surface of a battery with a total thickness of 1,600 μm. They identified copper foil (anode surface) with a thickness ratio of approximately 6.25 % and copper powder (on the cathode and anode surfaces) with a thickness ratio of approximately 1.25 %. Gitis [159] studied electrode defect detection in coatings, utilizing Lamb waves to identify electrode scratches and cracks with lengths as short as 2 mm. Additionally, the integration end values of guided wave signals increase in the cathode and decrease in the anode in the presence of interlayer gaps and adhesion defects.

Overall, AE technology can determine the timing of electrode fracture during the electrochemical evolution process of LiBs, but most studies focus on half-cells. UT technology provides high-resolution visualization of surface defects and impurities, can locate small internal defects, and monitor the evolution of electrode material properties to a certain extent. However, there is still significant room for improvement in terms of resolution and detection speed.

4.2. Internal gassing

During cyclic aging, LiBs can experience internal gassing, leading to a reduced lifespan [160,161]. Conversely, gas generation during cycling processes reduces lithium-ion conductivity, increasing internal resistance [162]. In both cases, the elevated internal pressure from gas generation may cause battery swelling, mechanical stress within electrodes, or severe gas leaks [163,164], negatively impacting LiB lifespan and reliability.

In the investigation of MH alloy electrode charge/discharge cycles by Didier-Laurent et al. [48], the authors linked AE signals with lower energy and longer rise time to hydrogen evolution reactions. Subsequently, Etiemble et al. [157] further investigated the evolution of AE signals associated with hydrogen release. Similarly, Matsuo et al. [43]

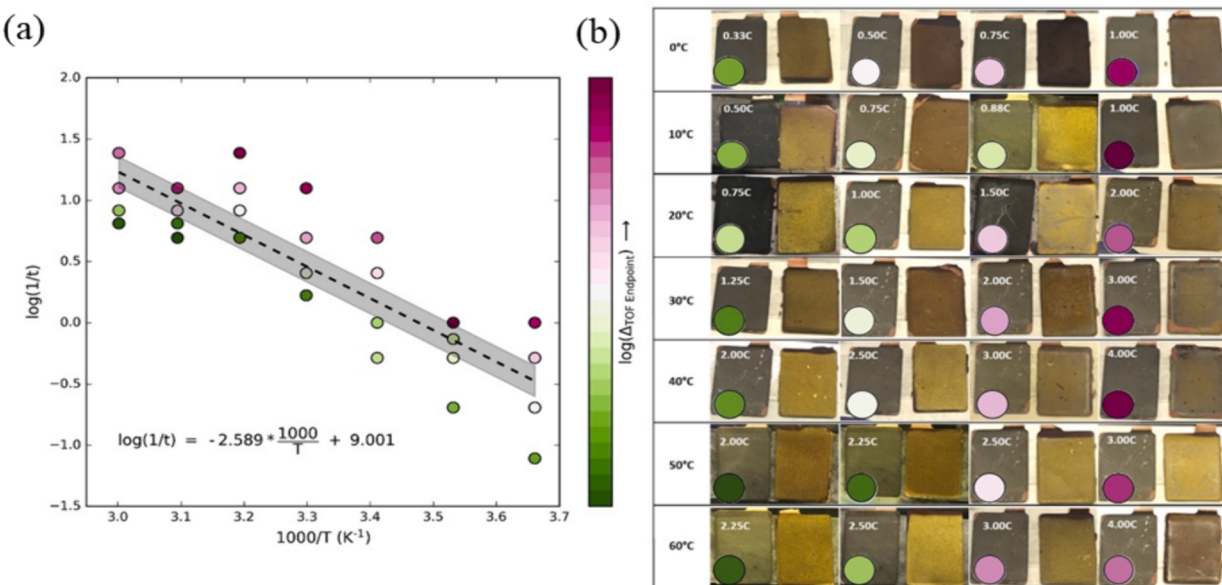


Fig. 7. Arrhenius relationship between plating, charging rate, and temperature [173].

continuously detected AE signals generated due to gas evolution in the battery.

Ultrasound faces considerable attenuation when encountering internal gas or voids within a battery, exhibiting scattering and reflection at gas–liquid interfaces. Some studies have successfully detected internal gas generation by analyzing ultrasound signals' attenuation and peak shift [52,165]. However, these approaches offer point detections, lacking a comprehensive analysis of gas generation throughout the entire battery. Li et al. [166] utilized air-coupled ultrasound sensors for C-scans on pouch cells with pore defects, characterizing pore location and shape in LiBs based on changes in ultrasound transmission signal energy amplitude. Huo et al. [73] mapped ultrasound transmission signal distribution in a solid-state LiB through planar scanning. The peak-to-peak value between the maximum and minimum signal amplitude of the recorded wave is converted into colors ranging from blue to red to create ultrasonic images. The motion module enables precise scanning in both horizontal and vertical directions with 0.2 mm accuracy, completing a 32 mm × 35 mm scan in approximately 300 s, as shown in Fig. 6, significant signal attenuation (deep blue) indicated gas presence. Xu et al. [59] improved signal-to-noise ratio using phased-array, employing full-matrix capture to collect signals. They employed the total focusing method to produce cross-sectional images, unveiling internal gas distribution, and simultaneously monitored gas evolution in LiBs across multiple cycles.

The introduction of ultrasound scanning and phased-array techniques has expanded the spatial and temporal scope of internal gassing. However, ultrasonic-based battery gas detection currently do not allow for high-precision three-dimensional imaging reconstruction of the internal gas distribution within the battery.

4.3. Lithium plating

Expanding the operational capabilities of LiBs to higher charging rates and a wider temperature range is highly desirable to enhance their applicability [167]. However, as mentioned earlier, LiBs can experience lithium deposition during processes such as low-temperature operation and high-rate charging. Excessive lithium deposition on the anode can result in the formation of solid-state lithium, leading to the occurrence of 'lithium plating (LP)' [168,169], significantly contributes to rapid capacity decay and the potential occurrence of thermal runaway [170,171].

Gold et al. [134] established a correlation between ultrasound signals and lithium intercalation in graphite electrodes, confirming ultrasound's potential for LP detection. Chang et al. [121], detected localized ultrasound signal variations during charging through two-dimensional scanning, attributing signal attenuation during fast charging to localized LP near the welding joint. However, it's noteworthy that acoustic signal loss can be attributed not only to LP but also to gas evolution [172]. Additionally, signal loss at low temperatures or high current rates may not be permanent, as demonstrated by recovery during return-point cycling [173]. Bommier et al. [173] conducted a series of measurements at temperatures ranging from 0 °C to 60 °C, with 10 °C increments, employing four different current rates at each temperature. The differences in Time of Flight (TOF) endpoints were calculated, and the cells were transferred to a glovebox after fixed capacity charging. Subsequently, they were disassembled at full State of Charge (SOC) for post-mortem characterization. They demonstrated the Arrhenius relationship between LP, current rate, and operating temperature. They established a significant correlation between ToF endpoint differences and graphite delamination, showing a stronger association with LP compared to methods relying solely on attenuated signals, as shown in Fig. 7. Currently, there is still limited research on ultrasound-based detection of LP in LiBs, distinguishing whether LP occurs on a single or multiple electrodes and identifying the impacted electrodes remains challenging.

4.4. Electrolyte infiltration

Adequate electrolyte impregnation is vital for LiBs to attain benefits such as high voltage and energy density [174,175]. In the battery manufacturing process, insufficient electrolyte injection directly impacts initial chemical reactions, resulting in reduced conductivity, heightened internal resistance, and shortened lifespan [176]. During battery usage, electrolyte loss occurs, and under harsh conditions, severe losses can happen. Once electrolyte loss reaches a critical level, it poses serious safety concerns [177–179]. Modestly increasing the electrolyte quantity aids in maximizing the utilization of active materials, but excessive electrolyte can promote side reactions, leading to the generation of substantial gas [180].

Deng et al. [62] conducted scans on pouch and prismatic LiBs using focused ultrasound beams, achieving sub-millimeter resolution. The experimental results indicated that ultrasound attenuated faster in

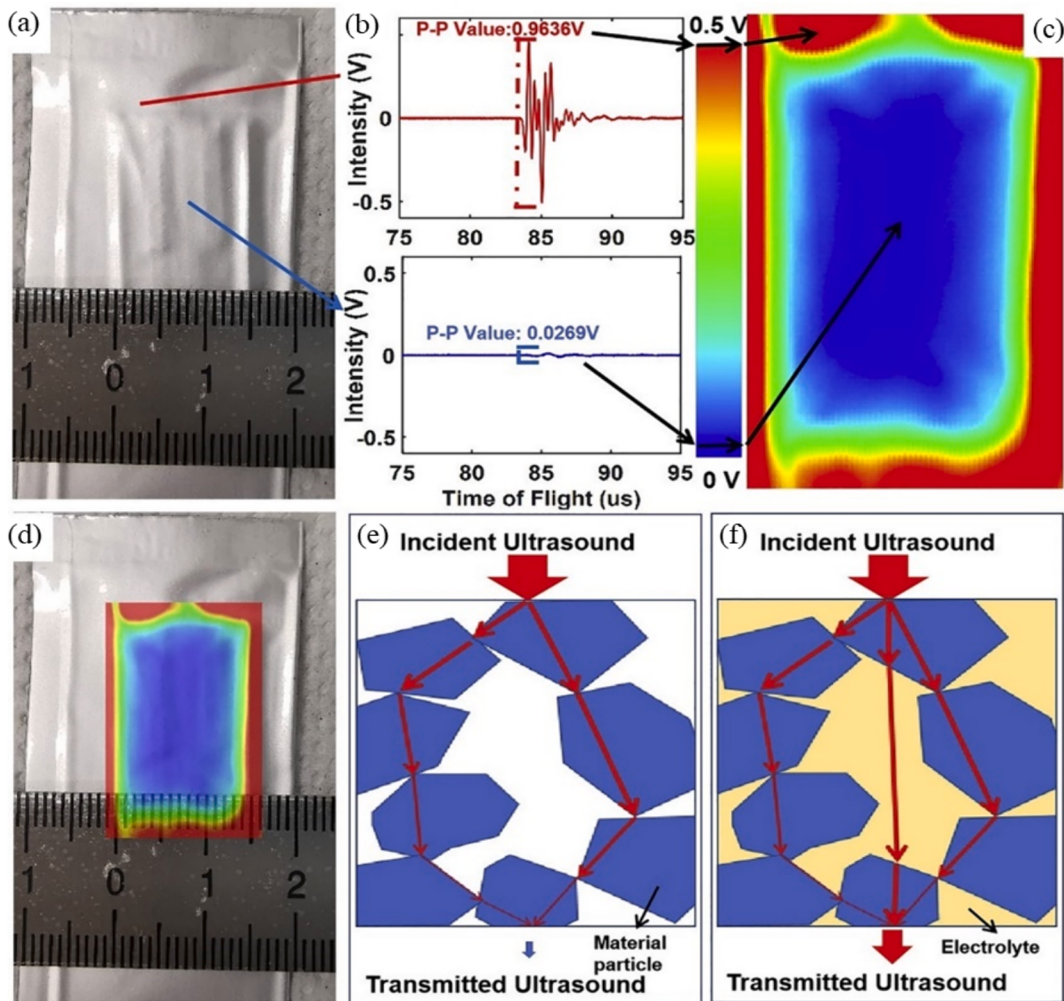


Fig. 8. Illustration of how ultrasonic waves are attenuated when gas or vacuum ss between electrode particles and how ultrasonic wanes transmit well when electrodes are well wetted with electrolyte [62].

electrodes or separators that were not sufficiently wetted compared to those that were adequately wetted, as shown in the Fig. 8. They successfully applied ultrasound imaging technology to observe the wetting process of cells and detected phenomena of electrolyte drying or “unwetting” due to cell expansion in both fresh and aged cells. However, their study was qualitative, focusing on the degree of electrolyte wetting without achieving an accurate evaluation of the electrolyte content. Hou et al. [63] prepared sample cells with different electrolyte contents, performed two-dimensional scans using an ultrasound probe, and obtained the distribution of transmission and reflection signals. They established a mapping relationship between the amplitude of ultrasound transmission signals and the electrolyte content in the battery, correcting the electrolyte content based on battery thickness information. This method achieved an error within 3 % for batteries with sufficient electrolyte content and maintained an error below 6 % even for batteries with lower electrolyte content.

Currently, electrolyte content measurement based on ultrasound scanning has found partial applications in industry. With further research and continuous technological advancements, this method holds the potential to significantly contribute to enhancing the production quality of LiBs.

Table 1 details the acoustic detection methods for lithium-ion battery material states and defects mentioned in Sections 4.1-4.4. In addition to detecting material states and defects, the operational status of lithium-ion batteries is a key indicator of dynamic performance. The next section will focus on the acoustic evaluation techniques for assessing

battery operational status.

4.5. State of charge

SoC, as one of the key state parameters of a battery, is crucial for ensuring the optimal performance, lifespan, and reliability of LiBs [40]. However, SoC cannot be directly measured but requires evaluation through the measurement of relevant physical quantities such as voltage, current, and temperature. SoC is defined as the ratio of the current capacity ($Q(t)$) to the nominal capacity (Q_n). Eq. (33) provides the mathematical definition of SoC [184,185]:

$$SOC(t) = \frac{Q(t)}{Q_n} \quad (33)$$

Despite the defined expression for SoC, accurately evaluating real-time SoC for LiBs remains challenging [43]. One reason is that the rated capacity (Q_n) of a battery can vary due to factors such as aging, temperature, self-discharge, and manufacturing differences. Additionally, the inconsistent internal performance and operating conditions of LiBs, often used in combination, undoubtedly increase the difficulty of assessing the overall performance of battery packs. Due to these unpredictable factors, attaining precise SoC assessment remains a complex task [186–188].

In recent years, a considerable amount of research has been conducted to optimize the accuracy of SoC evaluation. This paper categorizes SoC evaluation methods into six classes from the perspectives of

Table 1

Summary of ultrasonic diagnosis for LiBs defects.

Author/Year	Battery type	Defect types	Signal mode	Coupling medium	Excitation frequency	Imaging mode	Advantages	Disadvantages
Bauermann, et al./2020 [54]	Button cell and pouch cell	Electrode cracks and wrinkles, internal gassing	Pulse-echo	Distilled Water	15 MHz	A-Scan	Cheap, convenient, and rapid	Inability to identify defect depth, inapplicability to Curved cell configurations
Appleberry, et al./2022 [181]	Pouch cell	Electrode Cracks, internal gassing	Transmit-receive	Rubber and Adhesive	500 kHz	/	Cheap, convenient, and rapid	Inability to quantitatively analyze defects
Yi, et al./2021 [58]	Pouch cell	Metal defects on electrodes	Pulse-echo & transmit-receive	Dimethicone	2.5 MHz	B-Scan, C-Scan and tomographic	Effectively visualizing defects.	Inability to provide accurate thickness and depth information.
Li, et al./2019 [166]	Pouch cell	Internal gassing	Transmit-receive	Air	400 kHz	C-Scan	Cheap, convenient, and rapid	Inability to identify defect depth
Deng et al./2020 [62]	Pouch cell and prismatic cell	Unwetting, internal gassing	Transmit-receive	Silicone oil	2 MHz	A-Scan	Cheap, convenient, and rapid	Poor generalizability
Wu et al./2019 [52]	Pouch cell	Internal gassing	Pulse-echo	Epoxy	1 MHz	/	Cheap, convenient, and rapid	Inability to visualize defect
Bommier et al./2020 [182]	Pouch cell	Silicon passivation	Transmit-receive	Ultrasonic gel	2.25 MHz	/	Cheap, convenient, and rapid	Poor generalizability
Shen et al./2023 [51]	Pouch cell	Internal gassing	Pulse-echo	Ultrasonic gel	5 MHz	A-Scan, 2D/3D TFM	Effectively visualizing defects.	Inapplicability to curved cell configurations
Bommier et al./2020 [173]	Pouch cell	Lithium metal plating	Transmit-receive	Ultrasonic gel	2.25 MHz	/	Cheap, convenient, and rapid	Inability to identify the individual electrode's contribution
Chang et al./2021 [121]	Pouch cell	Lithium metal plating	Transmit-receive	Mineral oil	2.25 MHz	A-Scan	Cheap, convenient, and rapid	Inapplicability to curved cell configurations
Pham et al./2020 [165]	Pouch cell	Internal gassing	Pulse-echo	Ultrasonic gel	2.25 MHz	/	Cheap, convenient, and rapid	Insufficient accuracy
Sun et al./2023 [183]	Pouch cell	Tension rupture	Transmit-receive	Ultrasonic gel	5 MHz	/	Cheap, convenient, and rapid	Insufficient accuracy

Table 2

Classification of SoC evaluation methods.

Methods	Categories	Accuracy	Real-time	Robustness	Cost	Advantages	Disadvantages
Non-model-based methods	Open-circuit voltage method [190], impedance method [191,192], coulomb counting method [193]	Low	Medium	Medium	Low	Ease of implementation, low computational cost	Susceptible to environmental influences, requires regular calibration
Model-based methods	Electrochemical model [194–197], electrochemical impedance model [198,199]	High	Medium	High	High	High adaptability and accuracy	Complex modeling, time-consuming, requires prior knowledge
Data-driven methods	Neural network [200,201], Long short-term memory [202], Support vector machine [203,204], Fuzzy Logic method [205,206]	High	High	Low	High	High nonlinear predictive ability, real-time capability, no prior knowledge required	High computational complexity, strong data dependency, poor interpretability
Hybrid methods	Electrochemical model & adaptive filter [207], coulomb counting method & electrochemical model [208]	High	High	High	High	High real-time performance, accuracy and robustness	Complex modeling, strong data dependency
Physical measurement	Thickness method [209,210]	Low	High	Medium	Low	High efficiency, low cost	Insufficient accuracy, poor robustness
Ultrasonic methods	Bulk wave-based method [69,70], Guided wave-based method[72,140]	High	High	Medium	Low	Ease of implementation, high efficiency and accuracy, low cost	Susceptible to environmental influences

models and data: non-model-based methods, model-based methods, data-driven methods, hybrid methods, physical measurement and ultrasonic methods. Table 2 prominently highlights the strengths, weaknesses, and characteristics of each method [185,187,189].

Non-model-based methods infer SoC by establishing mapping relationships between external static parameters of the battery (such as open-circuit voltage, real-time current, impedance) and SoC. This method tends to have lower accuracy and may require regular calibration in practical applications. Model-based methods involve modeling

battery behavior using mathematical approaches to simulate electrical, chemical, or their combined processes, achieving accurate SoC evaluation. While model-based methods offer good accuracy and robustness, they demand substantial prior knowledge. Data-driven methods rely on the analysis of extensive testing data and nonlinear relationships between SoC and various parameters using sophisticated deep learning or machine learning frameworks. Hybrid methods, combining multiple algorithms, significantly enhance SoC evaluation accuracy and robustness. Furthermore, physical measurement methods associate changes in

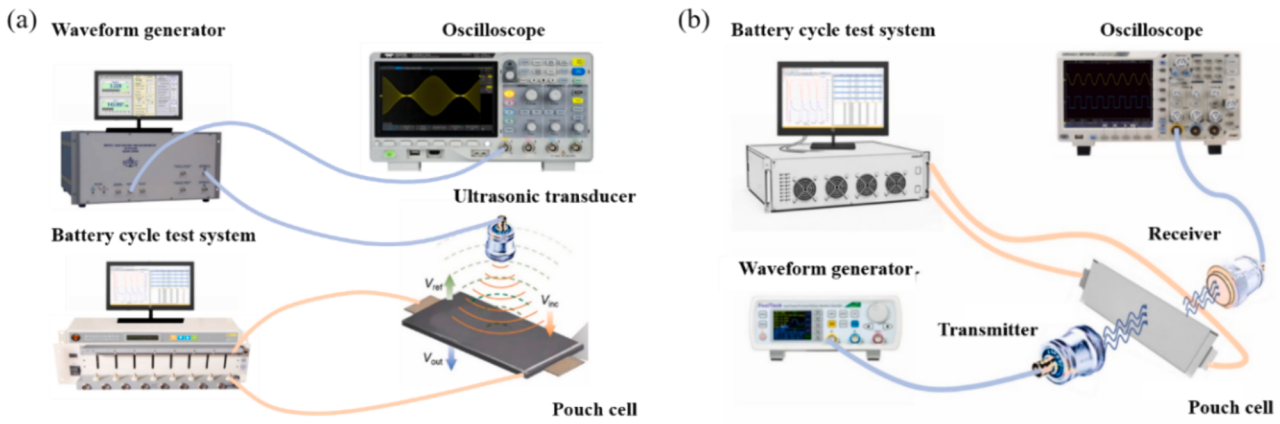


Fig. 9. (a) Schematic of pulse-echo mode. (b) Schematic of transmission mode [71].

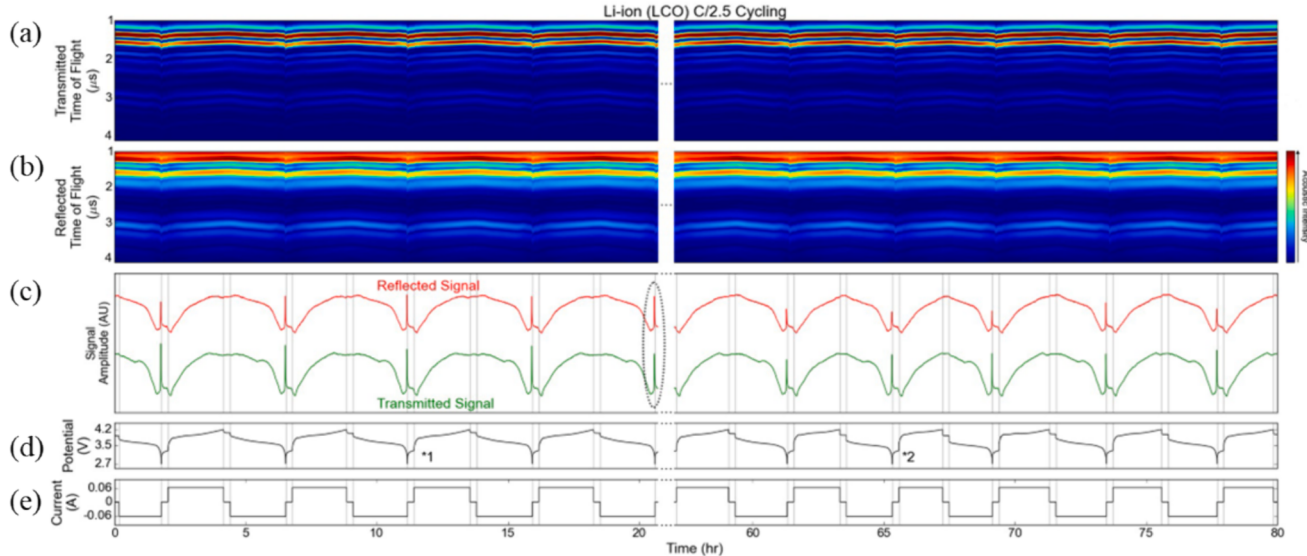


Fig. 10. Acoustic characteristics of LiCoO_2 /graphite cylindrical battery, where (a, b) depict the transmitted acoustic signals and reflected acoustic signals, respectively, during multiple cycles of the LiCoO_2 pouch cell, (c) illustrates the variation in SA for both reflected and transmitted signals during the battery charge (voltage increase)-discharge(voltage decrease) cycling process, and (d, e) represent the changes in battery potential and current during the charge-discharge cycling of the battery [69].

thickness and other physical dimensions with SoC, and while they are easy to implement, they suffer from shortcomings in terms of accuracy and robustness.

However, the aforementioned methods primarily rely on external measurements of voltage, current, and temperature, neglecting the changes in the internal properties of the battery as SoC varies. Ultrasonic methods have become one of the most promising approaches for battery SoC assessment due to their advantages such as low cost, non-invasiveness, and high sensitivity. By analyzing the propagation of stress waves in the battery, this method can continuously monitor the performance, internal structure, and state of LIBs [71,142].

4.5.1. Evaluation based on bulk waves

The ultrasonic method based on bulk waves mainly includes two modes: (1) Pulse-echo mode, where a single transducer is responsible for emitting sound waves and receiving reflected signals; (2) Transmission mode, where two transducers located on either side of the battery emit and receive signals [14,211], as illustrated in Fig. 9.

Hsieh et al. [69] initially demonstrated the feasibility of ultrasonic-based SoC evaluation from a theoretical standpoint. They employed a composite homogenization model to simulate the internal structure of

LIBs, and through Clawpack-Dualfoil simulations [212,213], they obtained variations in ultrasonic behavior during battery cycling. Additionally, they collected ultrasonic reflection and transmission signals from LiCoO_2 /graphite batteries. As shown in Fig. 10, during the initial stage of charging process (voltage increase), the modulus and density of the LiCoO_2 cathode undergo changes due to phase transitions, resulting in a slight decrease in SA. Subsequently, the SA steadily increases with the increase in SoC, and at the end of charging, a slight increase in ultrasound absorption is observed due to the biphasic reactions occurring at the cathode. Davies et al. [70] obtained similar experimental results, attributing the continuous increase in wave velocity during the charging process to the rapid elevation of the anode modulus and the reduction in electrode density [212,213–215]. Chang et al. [216], Robinson et al. [217], Kim et al. [53], and Sun et al. [183] noted a notable and prolonged reduction in ultrasound absorption at discharge initiation, interpreting it as a compliance change associated with Li gradient distribution within cathode particles. The above-mentioned studies demonstrate a clear and reproducible mapping relationship between battery cycling behavior and ultrasonic waveforms.

As research advances, an increasing number of scholars seek to quantitatively characterize SoC through specific features within

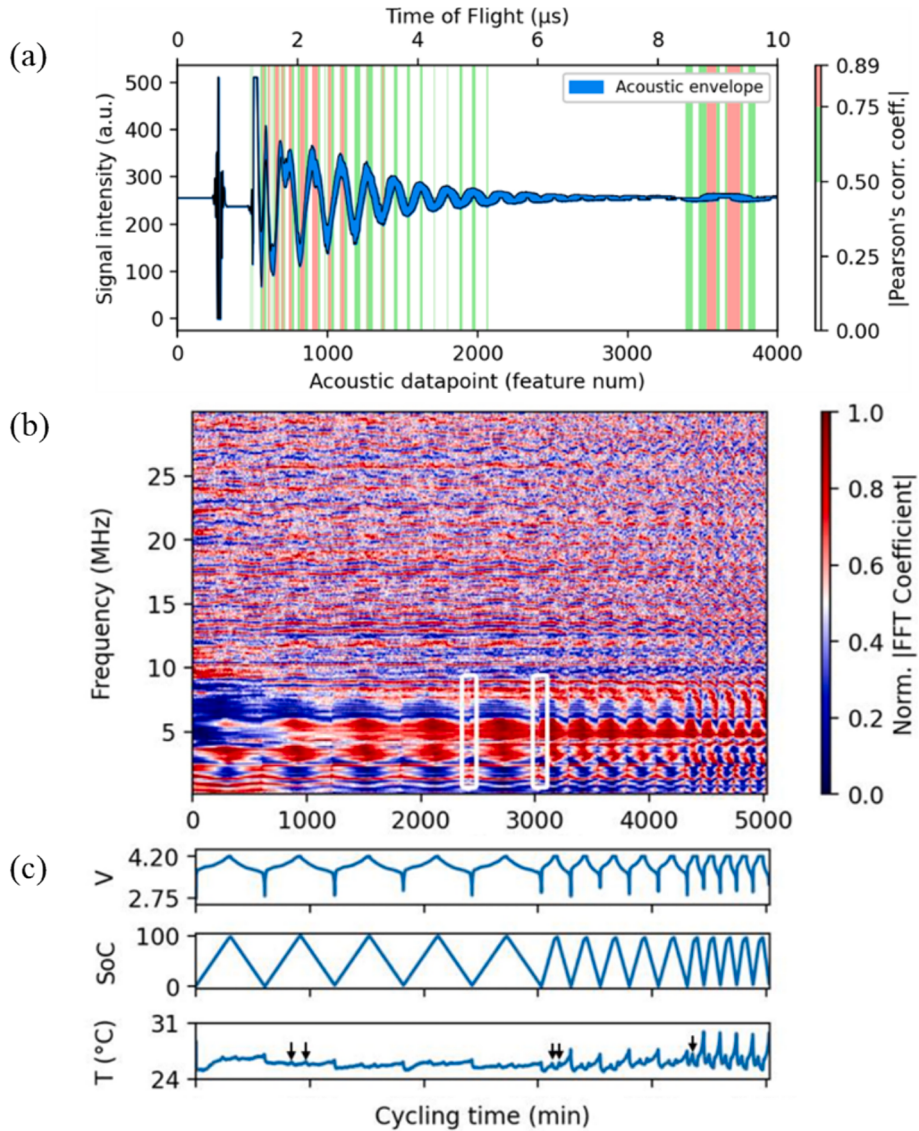


Fig. 11. Galiounas et al.'s experimental test results, (a) acoustic envelopes of all recorded waveforms. The background shading represents the Pearson correlation of each acoustic data point with SoC. (b) Presents a time-domain color map, with white rectangular boxes indicating occurrences of abrupt changes. (c) Illustrates the variations in voltage, SoC, and temperature throughout the experiment. Five cycles with rates of C/5, C/2, and 1C can be distinguished based on their duration. Examples of mid-SoC temperature peaks are indicated by arrows [142].

ultrasonic signals. Biot's theory, as applied by Gold et al. [134], characterizes LiBs by demonstrating that the use of "relatively low" frequencies leads to the generation of two longitudinal waves. Through experimentation, a discernible linear relationship between the slow wave's SA and SoC was identified. Leveraging this correlation, they successfully attained a quantitative representation of SoC. Davies et al. [70] employed the support vector regression to extract ToF shift and total signal amplification from ultrasonic signals, thereby enhancing the evaluation accuracy of SoC. Copley et al. [120] argued that the robustness and adaptability of inference methods relying on specific acoustic peaks or peak envelopes could be significantly affected by external environmental factors. They developed an intelligent peak selection method based on cross-wavelet transform, identifying signal regions with optimal battery charging correlation to optimize assessment. Ke et al. [141] analyzed commercial LiBs under varying temperatures, confirming that material properties and temperature exert less influence on the SA compared to ToF in ultrasonic signals. Meng et al. [71] quantitatively characterized SoC using ultrasonic damping in frequency-domain analysis, yielding precise frequency-domain

representation and high robustness. Huang et al. [136] employed a slurry model to construct electrode models and utilized ultrasonic resonance methods to achieve structured SoC tracking and evaluation during charging cycles. Galiounas et al. [142] utilized feedforward neural networks (FNN) to individually train on (1) the entire signal waveform (Fig. 11a), (2) waveform features extracted through Pearson correlation thresholding (Fig. 11a), and (3) Fourier coefficient amplitudes in the frequency domain (Fig. 11b). In all cases, they achieved satisfactory evaluation accuracy. Cai et al. [218] applied empirical mode decomposition for denoising and signal reconstruction, using the Hilbert transform to extract the maximum instantaneous energy of ultrasonic signals for SoC assessment. Wei et al. [219] proposed evaluating battery SoC using the initial rise time. Huang et al. [220] utilized global focusing scanning technology for ultrasonic signal collection and applied a deep learning algorithm based on FNN to analyze ultrasonic waves. This approach enabled in-situ SoC detection with high spatial resolution, particularly for pouch batteries. Table 3 provides a detailed summary of bulk wave-based SoC monitoring methods.

Table 3

Summary of SoC evaluation based on bulk waves.

Author/Year	Test mode	Excitation frequency	Feature extraction	Evaluation error	Advantages	Disadvantage
Hsieh et al./ 2015 [69]	Pulse-echo & transmit-receive	2.25 MHz	ToF and sum of SA	/(Qualitative analysis)	Convenient and cost-effective	Inability to conduct quantitative analysis, poor robustness
Gold et al./ 2017 [134]	Transmit-receive	200 kHz	ToF and SA	3.5 %	Capable of quantitative analysis	Susceptible to environmental influences
Davies et al./ 2017 [70]	Transmit-receive	2.25 MHz	ToF shift and total signal amplify	1 %	High accuracy	Insufficient generalization
Chang et al./ 2019 [216]	Transmit-receive	400 k	SA	/	Simple deployment, low cost	Low signal-to-noise ratio
Copley et al./ 2021 [120]	Pulse-echo	2 MHz	ToF	/	Strong robustness	Inability to perform quantitative analysis
Ke et al./2022 [141]	Pulse-echo	2.5 MHz	SA	/	Incorporates considerations for temperature and charging rate effects	Inability to perform quantitative analysis
Meng et al./ 2022 [71]	Transmit-receive	0.5 ~ 3.5 MHz	Dissipation coefficient	5 %	High robustness and efficiency	Complexity in modeling
Huang et al./ 2022 [136]	Pulse-echo	5 MHz	Resonant frequency	1 %	SoC assessment with layer resolution	Contact-based detection, bulky probe
Huang et al./ 2023 [220]	Transmit-receive	1 MHz	Raw signal	3.02 %	Capable of localized SoC evaluation	Poor interpretability

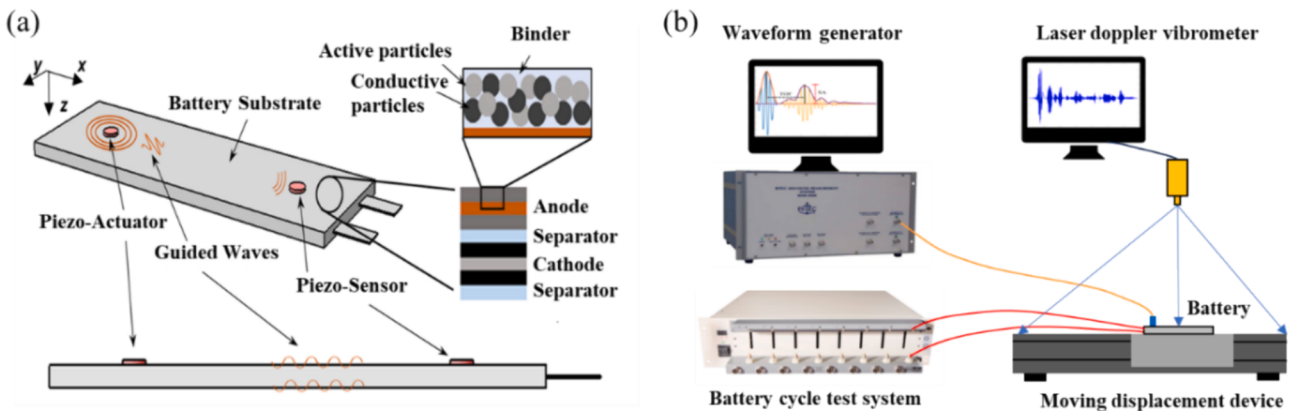


Fig. 12. (a) Illustrates a schematic diagram of a dual transducer guided wave detection device, concurrently representing the layered internal structure and materials of the battery [72]. (b) Depicts a schematic diagram of an UGW scanning experimental system.

4.5.2. Evaluation based on guided waves

Guided wave evaluation methods predominantly utilize the pitch-catch mode, employing two dedicated transducers for emitting and receiving ultrasonic signals [14,211], as depicted in Fig. 12 (a). In addition, there is a method employing an UGW scanning system to measure the micro-displacement of the battery surface, thereby obtaining guided wave signals, as depicted in Fig. 12b [221].

Ladpli et al. [72,140] introduced a pioneering approach utilizing built-in ultrasonic transducers to achieve real-time SoC evaluation. An example signal is depicted in Fig. 13a. In Fig. 13b and c, it can be observed that there is a significant non-linear relationship between time-domain signal characteristics and SoC. They attributed this to the intercalation stages in the graphite anode, coupled with concentration limitations in the cathode. They clearly identified the battery's phase transition characteristics using the first derivatives of voltage and ToF with respect to battery capacity (see Fig. 13d) [122,213,215]. It is noteworthy that they did not use voltage as a covariate but delved into the isolated acoustic properties for the assessment of the battery's state.

Ladpli et al. [222] proposed an efficient UGW feature extraction method using matching pursuit. This technique decomposes complex waveforms into linear components, aligning with the original signal structure via a Gabor dictionary to extract valuable time-frequency information [223]. Combining Gabor parameters with voltage data enhances SoC statistical evaluation accuracy. Popp et al. [224] explored the impact of temperature and charging rate on ToF, enhancing evaluation robustness by incorporating temperature parameters as

compensatory information. Zhao et al. [225] and Liu et al. [226] employed a scanning laser Doppler vibrometer for rapid guided wave signal capture. Through comprehensive multi-angle analysis in the time, frequency, and time-frequency domains, they significantly improved the efficiency of guided wave detection in LiBs production lines. Liu et al. [226] employed a two-dimensional Fourier transform on guided wave signals from array scanning experiments. They associated the dispersion phenomenon with SoC by generating frequency-wavenumber maps under different SoC conditions. They observed that with decreasing SoC, the relaxation of interlayer structures due to lithium ion deintercalation at the graphite anode led to the gradual prominence of the A mode dominated by out-of-plane displacement. Additionally, Li et al. [227] employed an adaptive FNN-XGBoost model to analyze multiple feature indicators in the time and frequency domains, achieving more precise assessment results. Table 4 summarizes the guided wave-based SoC evaluation methods.

4.6. State of health

The state of health (SoH) of a battery is a path-dependent parameter associated with aging and cannot be directly measured, thus lacking a unified definition [228]. Most researchers define SoH based on capacity or impedance, expressed mathematically as follows:

$$SoH_E = \frac{Q_{aged}}{Q_{fresh}} \quad (34)$$

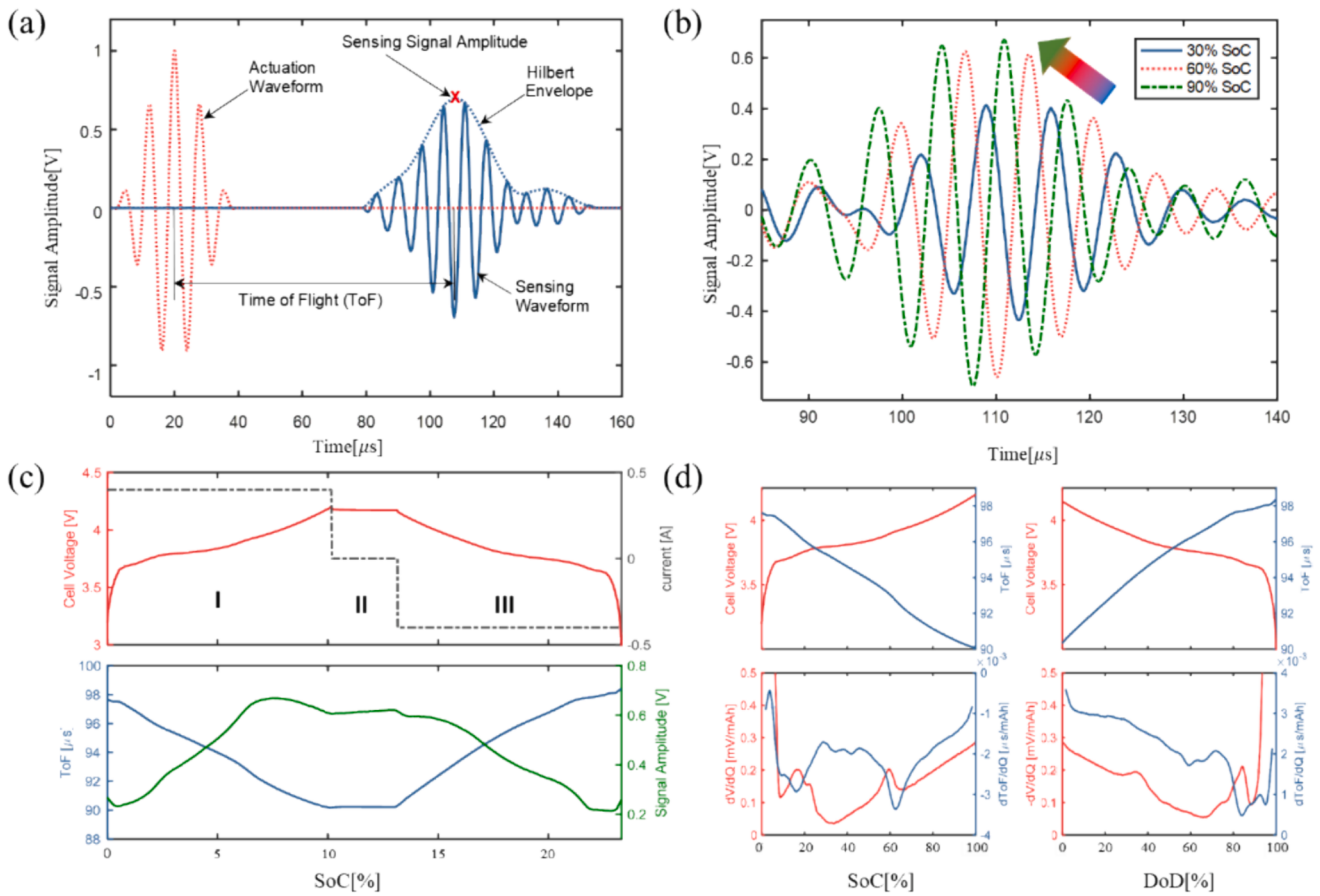


Fig. 13. (a) Illustrates representative signals from the transducer pair, defining ToF and SA. (b) Guided wave signal changes during a charging cycle with SoC variations, indicating the leftward and upward shift of the wave packet with increasing SoC. (c) Depicts the evolution of current and voltage data during a charging cycle, along with changes in ToF and SA. (d) Visualizes the first derivatives of voltage and ToF concerning battery capacity during charge and discharge cycles [140].

Table 4
Summary of SoC evaluation based on guided waves.

Author/Year	Sensor type	Excitation frequency	Feature extraction	Analysis method	Evaluation error	Advantages	Disadvantages
Ladpli et al./ 2017[140]	Piezo	125 kHz	ToF/SA	/	/	Convenient and cheap	Inability to conduct quantitative analysis
Ladpli et al./ 2018[222]	Piezo	125 kHz	Gabor parameters	GAMs	0.55 %	High precision	Temperature factors not taken into account
Ladpli et al./ 2018[72]	Piezo	125 kHz	ToF/SA	Statistical analysis	0.5 %	High precision	Lack of theoretical analysis
Popp et al./ 2018[224]	Piezo	30 kHz	ToF	Mean fitting	1.29 %	Considering temperature influence	Inability to compensate for significant changes in mechanical behavior
Zhao et al./ 2021[225]	Laser	90–120 kHz	ToF/SA/Power spectral density	Linear regression	/	Non-contact, large detection area and high efficiency	Lack of theoretical analysis
Gao et al./ 2022[152]	Piezo	500 kHz	Frequency-wavenumber spectrum	/	/	Theoretical model construction	Inability for quantitative analysis, lack of experimental validation.
Liu et al./ 2022[226]	Laser	100–200 kHz	SA/ToF	Neural network	3.76 %	Non-contact and high efficiency	Data dependency.
Li et al./2022 [221]	Laser	125 kHz	EIT and KurtosisC	Random forest	9.49 %	Non-contact and high efficiency	Experiment poses challenges with low precision
Li et al./2022 [227]	Piezo	25–200 kHz	Extracted features	FNN-XGBoost	2.36 %	Simultaneous detection of adverse reactions	Data dependency
Gao et al./ 2023[150]	Piezo	150 kHz	Group velocity(A0)	Numerical analysis	4 %	Applicable to multiple types of batteries	Temperature factors not taken into account

$$SoH_p = \frac{R_{EOL} - R_{aged}}{R_{EOL} - R_{fresh}} \quad (35)$$

where Q_{fresh} represents the nominal capacity of the battery in its latest

state, Q_{aged} is the capacity of the battery in an aged state. R_{fresh} denotes the internal resistance of the battery in its latest state, R_{EOL} is the internal resistance at the end of battery's life, and R_{aged} is the aging internal resistance measured at a specific time point in the battery's life.

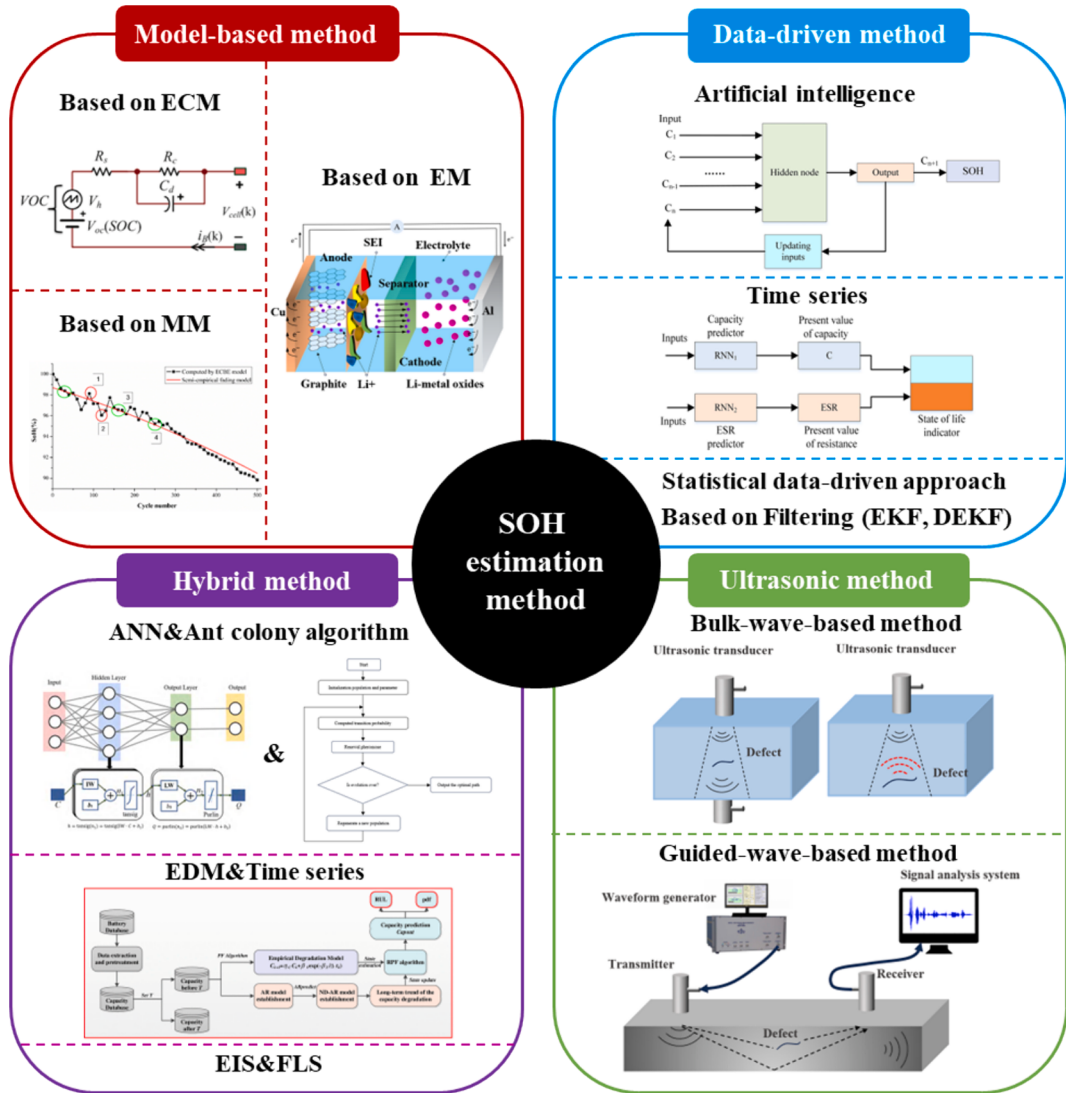


Fig. 14. Summary of SoH evaluation methods [237,232,233,235,236].

However, in the early stages of battery aging, there may be no clear increase in internal resistance or decrease in capacity, suggesting traditional definitions may not fully capture internal aging mechanisms [229]. Therefore, some researchers utilize relevant aging mechanism parameters to characterize the SoH of batteries [230,231]. In recent years, researchers have developed numerous SoH evaluation methods, broadly categorized into four types: model-based methods, data-driven methods, hybrid methods, and ultrasonic methods, as shown in Fig. 14.

Model-based approaches, including ECM-based, electrochemical model-based, and mathematical model-based methods [231–233], abstractly model battery aging behavior by simulating SoH using electrical or electrochemical characteristics. These methods require substantial prior knowledge for modeling. In contrast, data-driven methods, while not requiring an analysis of the battery aging process, rely on extensive data for continuous model optimization [234]. Hybrid methods, integrating various algorithms, aim to combine the strengths of both approaches for improved SoH evaluation accuracy and robustness. However, they face challenges related to high computational complexity [235,236]. Additionally, novel methods such as SoC-based, incremental capacity-based, and ultrasound-based approaches offer distinct advantages, expanding the range of SoH evaluation approaches.

UT is widely employed in the SoH assessment of batteries due to its non-destructive nature, low cost, and high sensitivity. Ultrasonic signals

demonstrate heightened sensitivity to internal material parameters in batteries, closely associated with the SoH. Consequently, for precise characterization of maximum capacity degradation when monitoring the SoH using ultrasonic signals, it is recommended to conduct assessments under full charge conditions [52].

Sood et al. [238] were among the first to employ ultrasonic detection for monitoring the degradation of LiBs. They attributed the primary cause of battery degradation to the increased internal pressure resulting from gas evolution, leading to electrode separation or damage. Bomnier et al. [182] employed a combined approach involving electrochemical and ultrasonic methods to monitor the entire aging process of LiBs. Hsieh et al. [69] gathered ultrasonic data from both pouch cells and cylindrical 18,650 cells, focusing on reflected and transmitted signals. Their findings revealed a progressive improvement in acoustic signals during full charge cycles. Notably, the study lacked a correlation analysis between acoustic behavior and SoH. Wu et al. [52], through a combination of ultrasonic signal analysis and data fusion, introduced the Spearman correlation coefficient to investigate the waveform evolution of ultrasonic reflected signals. They observed a stronger correlation between ToF and SoH in comparison to SA. Knehr et al. [239] integrated electrochemical impedance spectroscopy (EIS) with ultrasonic techniques. They observed ToF of the ultrasonic signal increases with increasing cycles. (see Fig. 15a,b). Subsequently, they correlated the

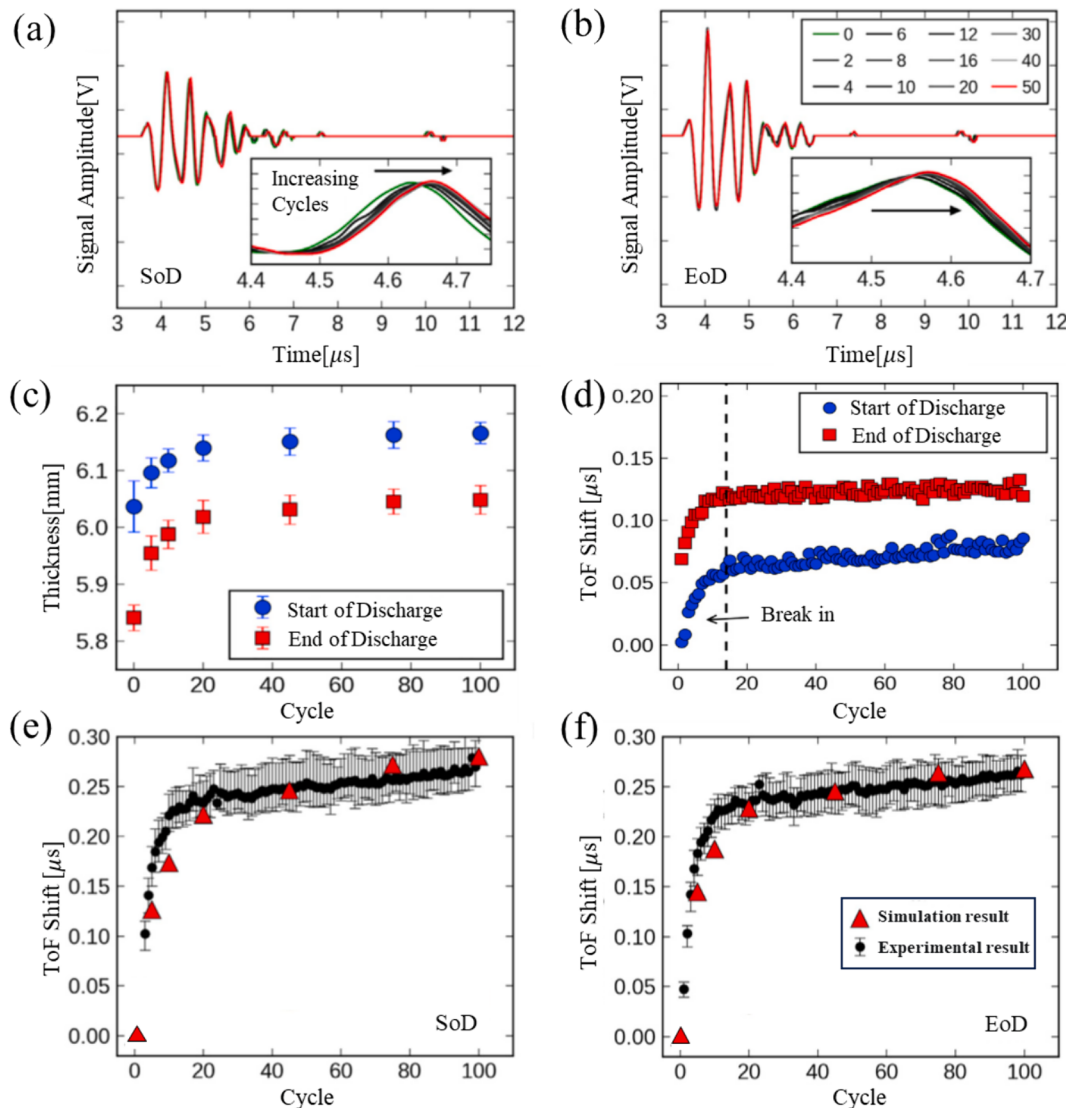


Fig. 15. Acoustic parameter variations during aging process of LiBs, (a) variations in ultrasonic signals during the discharge initiation along the cycling process (green represents recordings at the beginning of cycles, while red corresponds to recordings after 50 cycles), (b) evolution of ultrasonic signals after discharge completion throughout the cycling process. (c) thickness variation of the battery during cycling. (d) ToF shifts during battery cycling. (e) ToF shifts at the onset of discharge. (f) ToF shifts at the conclusion of discharge [239]. (For interpretation of the references to color in this figure legend, the reader is referred to the web version of this article.)

variations in effective modulus and battery thickness (see Fig. 15c) with Time of Flight (ToF) (see Fig. 15d). Theoretical calculations and experimental results exhibited good agreement (see Fig. 15e,f). This approach offers a methodological insight into studying the early-stage behavior of LiBs.

As research advances, more researchers are attempting to quantitatively characterize SoH. Davies et al. [70], for instance, combined key indicators from ultrasonic signals with voltage and, using the Support Vector Regression method, achieved an average error within 1.6 %. Li et al. [221] employed a scanning laser Doppler vibrometer to acquire guided wave signals on the battery's surface, observing a rapid decay in signal energy as the battery aged. Three custom-defined "line parameters" were selected, enabling a SoH assessment with an estimated error of 0.8 %. However, this approach may lead to anomalous evaluations of increasing SoH during the battery aging process. Zhao et al. [225] conducted a comparative analysis of signals in the time domain, frequency domain, and time-frequency domain at multiple central frequencies, enriching evaluation indicators. Ladpli et al. [72] observed that with an increase in the number of cycles, the guided wave velocity

gradually decreased. Moreover, significant peaks in ToF shifts were evident at the conclusion of discharge and the onset of charging (refer to Fig. 16a,d). Simultaneously, the attenuation of signals progressively diminished with an increase in cycle depth, with this effect being most pronounced at the end of charging (refer to Fig. 16b,e)). Utilizing a generalized additive model, they achieved remarkable results in evaluation with an average error of approximately 0.006 %. Table 5 summarizes the ultrasound-based assessment methods for SoH.

In conclusion, ultrasound-based detection methods are widely used for defect detection and state assessment in lithium batteries. However, different ultrasound techniques have unique strengths and limitations in comprehensive battery detection. This study reviews the optimal applications and respective advantages and disadvantages of three ultrasound methods (see Fig. 17), with the aim of providing a reference for future researchers in making informed selections.

5. Prospects for future directions

Ultrasound-based methods offer distinctive advantages in battery

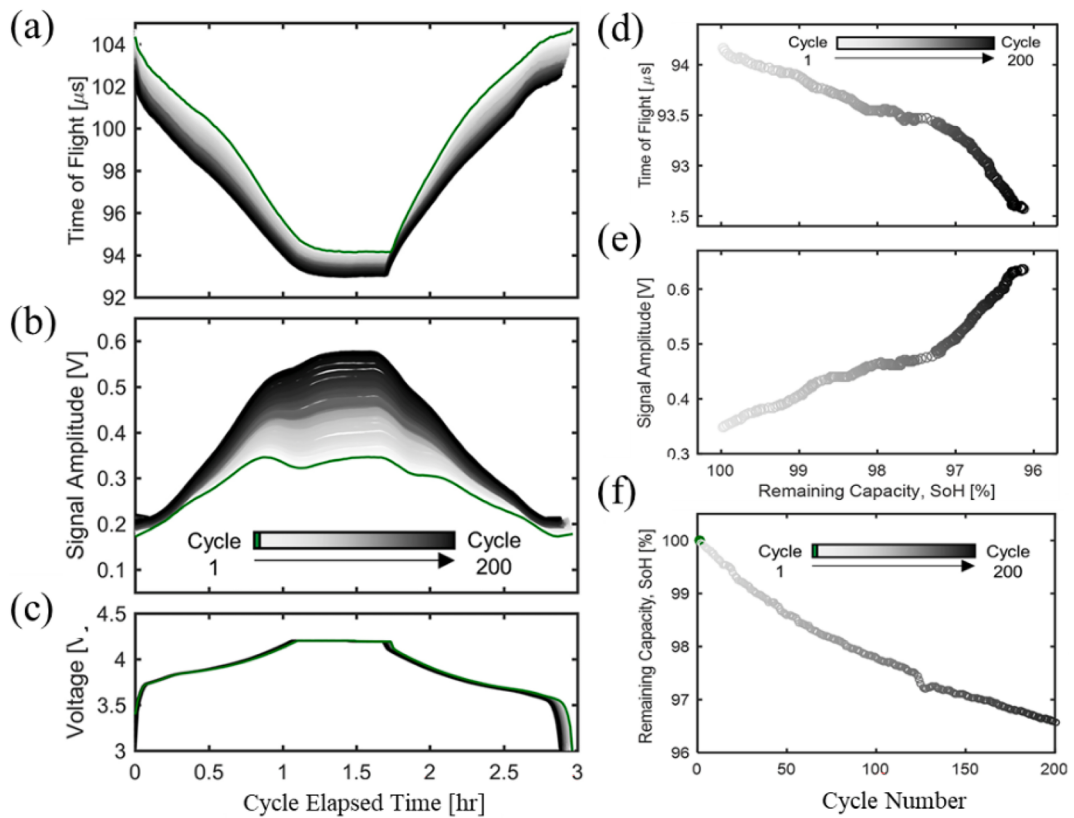


Fig. 16. (a) Evolutionary process of ToF, (b) SA, and (c) voltage across cycles, (d) Functional relationship of ToF, (e) SA, and (f) capacity with respect to SoH across cycles [72].

Table 5
Summary of ultrasonic assessment methods for SoH.

Author/Year	Ultrasound type	Test mode	Excitation frequency	Evaluation error	Advantages	Disadvantages
Hsieh et al./2015[69]	Bulk wave	Pulse-Echo & Transmit-Receive	2.25 MHz	/ (Qualitative analysis)	Pioneered the link between SoH and acoustic signals	No quantitative analysis conducted
Wu et al./2019 [52]	Bulk wave	Pulse-Echo	1 MHz	/	Linking SoH and ToF	No quantitative analysis conducted
Davies et al./2017[70]	Bulk wave	Pulse-Echo	2.25 MHz	1.9 %	High accuracy, single-measurement sufficiency, and strong generalization.	Not accounting for factors such as temperature.
Ladpli et al./2018[72]	Guided wave	Transmit-Receive	125 kHz	0.006 %	Multi-feature analysis, easy deployment and high accuracy	Single-feature and poor robustness
Knehr et al./2018[239]	Bulk wave	Pulse-Echo	2.5 MHz	/	Coupling diverse methods for robustness	No quantitative analysis conducted
Li et al./2022 [221]	Guided wave	Transmit-Receive	125 kHz	0.8 %	High stability and efficiency	Decreased evaluation accuracy with battery aging

damage detection and state assessment, showcasing considerable potential. However, they currently encounter limitations. This section provides a prospective outlook on future research (see Fig. 18), exploring topics like three-dimensional high-resolution imaging, study on aging mechanisms based on multi-modes ultrasonic signal analysis, online real-time monitoring system, parameter mapping from individual to pack and multi-factor corrective comprehensive diagnosis of LiBs based on ultrasonic detection.

5.1. 3D high-resolution imaging

Traditional 3D imaging algorithms encounter challenges in acquiring material information within batteries due to the presence of multiple layers of heterogeneous structures and the complexity of sound reflection paths. Future research could explore two approaches: deploying a full-sphere sensor array for comprehensive internal signal capture in

batteries and utilizing optimization algorithms, such as deep learning, for achieving 3D imaging (see Fig. 18). Additionally, the full-focus ultrasound 3D imaging method, initially applied in composite materials, could be adapted for lithium-ion battery research to obtain internal state information in three dimensions. In practical deployments of sensors, attention must be paid to the varying shapes of lithium battery surfaces, which pose challenges for rigid sensors to conform properly. Consequently, designing flexible global sensors for three-dimensional imaging of lithium batteries could be a future development direction. In actual deployments, the layout of global sensors may be constrained by the internal structure of the battery, and a trade-off must be made by allocating a portion of the battery's energy consumption to the sensor array. Additionally, it is essential to consider the impact of external interference and environmental condition changes.

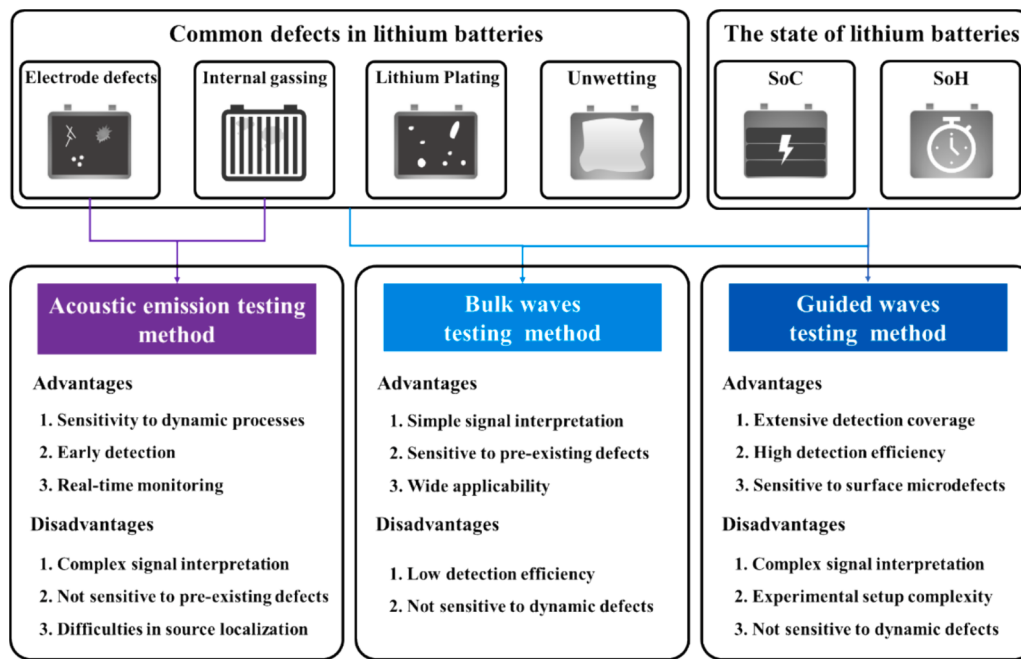


Fig. 17. Optimal Applications and Advantages and Disadvantages of Ultrasound-based Methods.

5.2. Study on aging mechanisms based on multi-modes ultrasonic signal analysis

Ensuring the longevity of LIBs and minimizing risks requires monitoring the entire aging process. Currently, ultrasonic-based methods are insufficient for comprehensive process monitoring, primarily due to the limited understanding of the aging mechanisms over the battery's entire lifecycle. Future research could attempt to achieve more precise evaluations of the battery aging process by comprehensively analyzing different types and modes of ultrasonic signals. This can be accomplished through acoustic signal analysis from multiple perspectives, including time domain, frequency domain, and time-frequency domain (as illustrated in Fig. 18). In practical applications, analyzing and processing multimodal ultrasonic signals undoubtedly consumes substantial time and computational power. Therefore, extracting highly correlated features is a critical step for the rapid and accurate characterization of battery aging behavior.

5.3. Online real-time monitoring system with integrated retirement management

Given the dynamic nature of modern manufacturing processes, the complexity of application environments, and the heterogeneity of battery states at the time of retirement, online real-time monitoring of LIBs' status is particularly crucial. Future research should focus on the development of lightweight monitoring methods to adapt to resource-constrained environments (energy, storage space, computational power, operation space, etc.), such as using handheld devices for data acquisition and processing. In practical applications, emphasis should be placed on developing simplified physical models or empirical models with low computational overhead. Data compression techniques should be employed to reduce the storage space and transmission bandwidth requirements of monitoring data. Utilizing low-power sensors and embedded systems will help reduce energy consumption and extend the lifespan of monitoring devices. When employing deep learning for data processing, techniques such as lightweight network architectures, pruning, quantization, and model compression need to be prioritized. In the development of this strategy, it is essential to continually achieve an optimal balance between accuracy and efficiency. The lightweight

characteristics will promote the adoption of acoustic monitoring methods in a broader range of applications, providing real-time capacity information and quality grading at the end of battery life, thereby helping to maximize battery lifecycle extension and alleviate recycling pressures and environmental pollution issues.

5.4. Parameter mapping from individual to pack

Current battery detection methods mainly focus on testing individual cells. In practical applications of battery-powered systems, multiple cells are typically connected in series or parallel to meet energy or power requirements, forming a battery pack. The evaluation of battery pack performance is complicated by factors such as temperature gradients and manufacturing variations, presenting new challenges. Future research can focus on developing embedded distributed detection systems, deploying monitoring sensors at multiple cell locations within the battery pack to capture internal temperature gradients and cell differences. Comprehensive analysis of these sensor data can provide the necessary support for accurately assessing the overall performance of the battery pack. Given the compactness and customization requirements of battery pack packaging, it is necessary to combine simulation and experimental methods to determine the optimal deployment locations and spacing for the distributed sensing system. Additionally, the battery pack design must accommodate local adjustments to facilitate sensor deployment and ensure the robustness of the deployment.

5.5. Multi-factor corrective comprehensive diagnosis of LIBs based on ultrasonic detection

Ultrasonic detection methods can proficiently characterize specific issues within LIBs, but there is potential for enhancement in terms of accuracy, robustness, and universality. Additionally, these methods fall short in providing comprehensive and timely assessment of all internal issues. Hence, a key research focus may involve signal integration, including voltage, temperature, geometric features, and impedance, as calibration factors for battery state assessment. Leveraging the data interpretation capabilities of machine learning and artificial intelligence technologies can extract high-value patterns and features from complex multi-parameter data, thereby enhancing accuracy and reliability. In

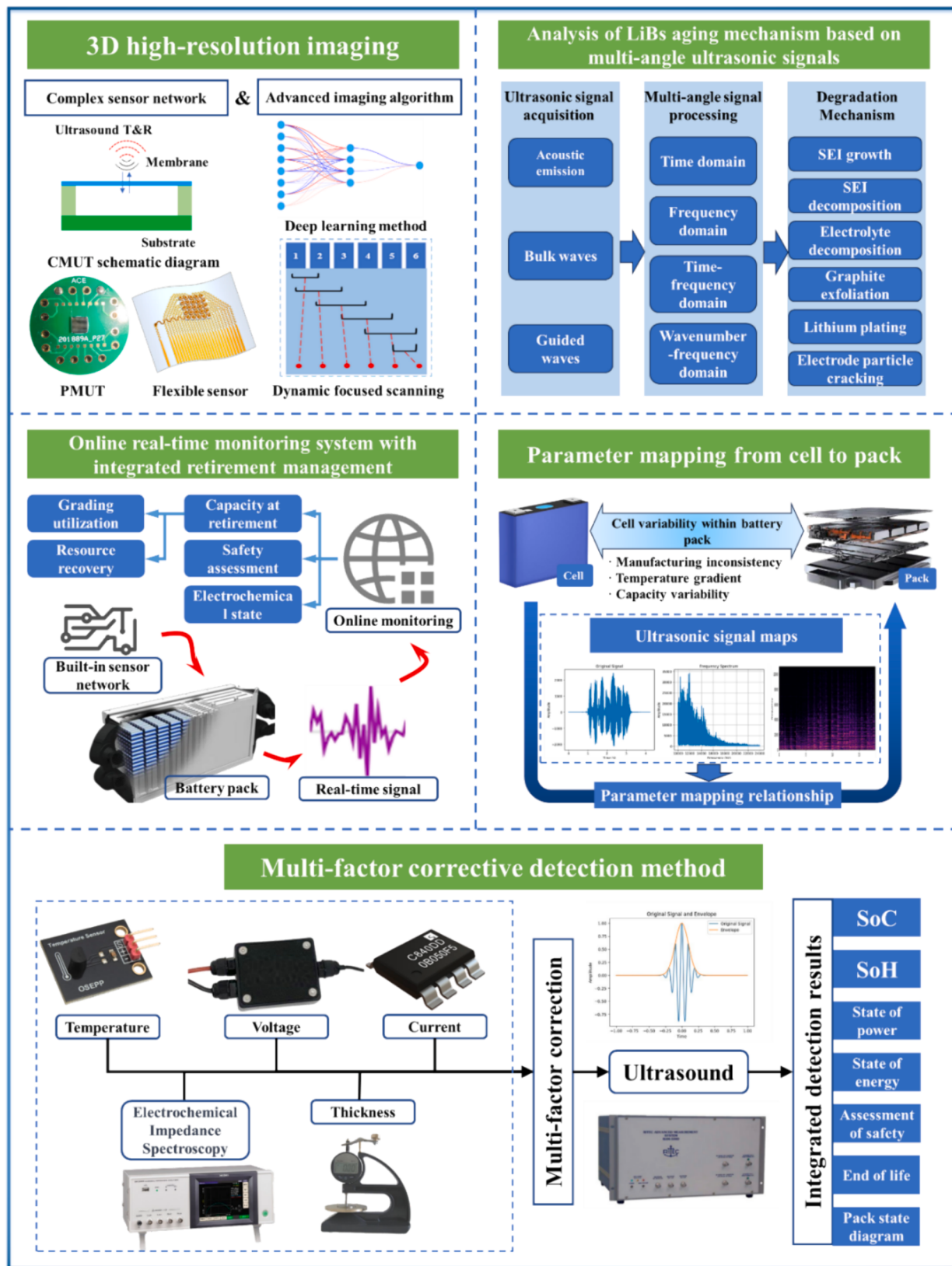


Fig. 18. Prospects for the future direction of ultrasonic detection in LiBs.

practical applications, integrating data from different sensors requires the development of data processing and integration technologies applicable to various data formats and transmission protocols. Extensive experimental validation and system testing are necessary to determine

the system's resistance to different conditions and interferences. Simultaneously, deploying and maintaining such a complex diagnostic system may entail high costs, including hardware, software, personnel, and training expenses.

6. Conclusion

This paper reviews ultrasound-based methods for monitoring the internal state evolution of LiBs. It addresses the in-situ monitoring demands arising from complex manufacturing processes and application scenarios. The paper discusses fundamental principles, providing a systematic overview of ultrasound-based methods applications in detecting various internal states of LiBs, including normal and slow electrochemical processes, aging, and abnormal failure processes. The conclusion offers a forward-looking perspective on emerging technologies for in-situ detection in LiBs.

A comprehensive review reveals that electrode particle fracture and gas generation from electrolyte decomposition are the main sources of AE in batteries, with distinct differences in the signals they generate. UT of batteries, including SoC, SoH, internal side reactions, and battery degradation, correlates with the attenuation and shift of ultrasonic signals. These correlations can be enhanced by considering other physical factors during battery evolution. Monitoring methods using ultrasound-based scanning techniques are effective in observing the global evolution process of LiBs, showcasing the potential applications of ultrasound-based detection technology in the in-situ detection field for LiBs.

This paper concludes by proposing some directions and possibilities for future research, including (1) 3D High-resolution imaging for LiBs, (2) multi-factor coupling monitoring method, (3) online real-time monitoring system for LiBs, (4) parameter mapping from individual to pack and (5) comprehensive monitoring of LiBs aging. By addressing these challenges and advancing research continuously, the potential of ultrasound-based technology can be better leveraged, thereby enhancing safety and efficiency at a higher level in the production, application, and recycling of LiBs. This, in turn, contributes to the further development of LiBs.

CRediT authorship contribution statement

Yaxun Gou: Writing – original draft, Investigation. **Yitian Yan:** Writing – original draft, Investigation, Conceptualization. **Yan Lyu:** Writing – review & editing. **Shili Chen:** Writing – review & editing. **Jian Li:** Writing – review & editing. **Yang Liu:** Writing – review & editing.

Declaration of competing interest

The authors declare that they have no known competing financial interests or personal relationships that could have appeared to influence the work reported in this paper.

Data availability

Data will be made available on request.

Acknowledgment

This work was supported in part by the National Science Foundation of China under contract number 61773283, in part by National Key R&D Program of China under contract number 2018YFC0808600.

References

- [1] D.Y. Voropaeva, E.Y. Safronova, S.A. Novikova, A.B. Yaroslavtsev, Recent progress in lithium-ion and lithium metal batteries, *Mendeleev Commun.* 32 (2022) 287–297.
- [2] K. Chayambuka, G. Mulder, D.L. Danilov, P.H. Notten, From li-ion batteries toward Na-ion chemistries: challenges and opportunities, *Adv. Energy Mater.* 10 (2020) 2001310.
- [3] M. Li, J. Lu, Z. Chen, K. Amine, 30 years of lithium-ion batteries, *Adv. Mater.* 30 (2018) 1800561.
- [4] G. Zubl, R. Dufo-López, M. Carvalho, G. Pasaoglu, The lithium-ion battery: state of the art and future perspectives, *Renew. Sustain. Energy Rev.* 89 (2018) 292–308.
- [5] B. Zhang, Y. Lyu, J. Gao, G. Song, Y. Zheng, Y. Lee, C. He, Ultrasonic characterization of multi-layered porous lithium-ion battery structure for state of charge, *Ultrasonics* 134 (2023) 107060.
- [6] A. Manthiram, An outlook on lithium ion battery technology, *ACS Cent. Sci.* 3 (2017) 1063–1069.
- [7] S. Hemavathi, Overview of cell balancing methods for Li-ion battery technology, *Energy Storage* 3 (2021) e203.
- [8] W. Xie, X. Liu, R. He, Y. Li, X. Gao, X. Li, Z. Peng, S. Feng, X. Feng, S. Yang, Challenges and opportunities toward fast-charging of lithium-ion batteries, *J. Energy Storage* 32 (2020) 101837.
- [9] V. Viswanathan, A.H. Epstein, Y.-M. Chiang, E. Takeuchi, M. Bradley, J. Langford, M. Winter, The challenges and opportunities of battery-powered flight, *Nature* 601 (2022) 519–525.
- [10] A. El Kharbachi, O. Zavorotynska, M. Latroche, F. Cuevas, V. Yartys, M. Fichtner, Exploits, advances and challenges benefiting beyond Li-ion battery technologies, *J. Alloy. Compd.* 817 (2020) 153261.
- [11] L. Qi, Y. Wang, L. Kong, M. Yi, J. Song, D. Hao, X. Zhou, Z. Zhang, J. Yan, Manufacturing processes and recycling technology of automotive lithium-ion battery: a review, *J. Storage Mater.* 67 (2023) 107533.
- [12] Y. Liu, R. Zhang, J. Wang, Y. Wang, Current and future lithium-ion battery manufacturing, *Iscience* 24 (2021).
- [13] E.M. Jin, M.S. Kim, T.Y. Kim, B.-J. Shin, J.-H. Moon, S.M. Jeong, Upcycling of silicon scrap collected from photovoltaic cell manufacturing process for lithium-ion batteries via transferred arc thermal plasma, *Energy* 262 (2023) 125447.
- [14] J.O. Majasán, J.B. Robinson, R.E. Owen, M. Maier, A.N. Radhakrishnan, M. Pham, T.G. Tranter, Y. Zhang, P.R. Shearing, D.J. Brett, Recent advances in acoustic diagnostics for electrochemical power systems, *J. Phys.: Energy* 3 (2021) 032011.
- [15] J. Schnell, C. Nentwich, F. Endres, A. Kollenda, F. Distel, T. Knoche, G. Reinhardt, Data mining in lithium-ion battery cell production, *J. Power Sources* 413 (2019) 360–366.
- [16] M.F.R. Zwicker, M. Moghadam, W. Zhang, C.V. Nielsen, Automotive battery pack manufacturing—a review of battery to tab joining, *J. Adv. Join. Process.* 1 (2020) 100017.
- [17] A. Kwade, W. Haselrieder, R. Leithoff, A. Modlinger, F. Dietrich, K. Droeder, Current status and challenges for automotive battery production technologies, *Nat. Energy* 3 (2018) 290–300.
- [18] F.M. Zanotto, D.Z. Dominguez, E. Ayerbe, I. Boyano, C. Burmeister, M. Duquesnoy, M. Eisentraeger, J.F. Montaño, A. Gallo-Bueno, L. Gold, Data specifications for battery manufacturing digitalization: Current status, challenges, and opportunities, *Batter. Superc.* 5 (2022) e202200224.
- [19] P.G. Balakrishnan, R. Ramesh, T.P. Kumar, Safety mechanisms in lithium-ion batteries, *J. Power Sources* 155 (2006) 401–414.
- [20] Y. Chen, Y. Kang, Y. Zhao, L. Wang, J. Liu, Y. Li, Z. Liang, X. He, X. Li, N. Tavajohi, A review of lithium-ion battery safety concerns: the issues, strategies, and testing standards, *J. Energy Chem.* 59 (2021) 83–99.
- [21] E. Kim, J. Song, C.B. Dzakpasu, D. Kim, J. Lim, D. Kim, S. Park, H. Lee, T.-S. Kwon, Y.M. Lee, Degradation behavior of 21700 cylindrical lithium-ion battery cells during overdischarge cycling at low temperatures, *J. Storage Mater.* 72 (2023) 108627.
- [22] X. Zhu, H. Wang, S. Allu, Y. Gao, E. Cakmak, E.J. Hopkins, G.M. Veith, Z. Wang, Investigation on capacity loss mechanisms of lithium-ion pouch cells under mechanical indentation conditions, *J. Power Sources* 465 (2020) 228314.
- [23] D. Ouyang, M. Chen, J. Liu, R. Wei, J. Weng, J. Wang, Investigation of a commercial lithium-ion battery under overcharge/over-discharge failure conditions, *RSC Adv.* 8 (2018) 33414–33424.
- [24] K. Qian, Y. Li, Y.-B. He, D. Liu, Y. Zheng, D. Luo, B. Li, F. Kang, Abuse tolerance behavior of layered oxide-based Li-ion battery during overcharge and over-discharge, *RSC Adv.* 6 (2016) 76897–76904.
- [25] N. Mao, T. Zhang, Z. Wang, Q. Cai, A systematic investigation of internal physical and chemical changes of lithium-ion batteries during overcharge, *J. Power Sources* 518 (2022) 230767.
- [26] G. Zhong, B. Mao, C. Wang, L. Jiang, K. Xu, J. Sun, Q. Wang, Thermal runaway and fire behavior investigation of lithium ion batteries using modified cone calorimeter, *J. Therm. Anal. Calorim.* 135 (2019) 2879–2889.
- [27] Q. Yuan, F. Zhao, W. Wang, Y. Zhao, Z. Liang, D. Yan, Overcharge failure investigation of lithium-ion batteries, *Electrochim. Acta* 178 (2015) 682–688.
- [28] M. Berecibar, I. Gandiaga, I. Villarreal, N. Omar, J. Van Mierlo, P. Van den Bossche, Critical review of state of health estimation methods of Li-ion batteries for real applications, *Renew. Sustain. Energy Rev.* 56 (2016) 572–587.
- [29] J. Lu, T. Wu, K. Amine, State-of-the-art characterization techniques for advanced lithium-ion batteries, *Nat. Energy* 2 (2017) 1–13.
- [30] P.P. Paul, E.J. McShane, A.M. Colclasure, N. Balsara, D.E. Brown, C. Cao, B.-R. Chen, P.R. Chinnam, Y. Cui, E.J. Dufek, A review of existing and emerging methods for lithium detection and characterization in Li-ion and Li-metal batteries, *Adv. Energy Mater.* 11 (2021) 2100372.
- [31] M. Crescentini, A. De Angelis, R. Ramilli, G. De Angelis, M. Tartagni, A. Moschitta, P.A. Traverso, P. Carbone, Online EIS and diagnostics on lithium-ion batteries by means of low-power integrated sensing and parametric modeling, *IEEE Trans. Instrum. Meas.* 70 (2020) 1–11.
- [32] M. Messing, T. Shoa, S. Habibi, Estimating battery state of health using electrochemical impedance spectroscopy and the relaxation effect, *J. Storage Mater.* 43 (2021) 103210.
- [33] Y. Yuan, K. Amine, J. Lu, R. Shahbazian-Yassar, Understanding materials challenges for rechargeable ion batteries with in situ transmission electron microscopy, *Nat. Commun.* 8 (2017) 15806.

- [34] H. Zhou, K. An, S. Allu, S. Pannala, J. Li, H.Z. Bilheux, S.K. Martha, J. Nanda, Probing multiscale transport and inhomogeneity in a lithium-ion pouch cell using *in situ* neutron methods, *ACS Energy Lett.* 1 (2016) 981–986.
- [35] D. Goers, M. Holzapfel, W. Scheifele, E. Lehmann, P. Vontobel, P. Novák, In situ neutron radiography of lithium-ion batteries: the gas evolution on graphite electrodes during the charging, *J. Power Sources* 130 (2004) 221–226.
- [36] M. Mohammadi, A. Jerschow, In situ and operando magnetic resonance imaging of electrochemical cells: a perspective, *J. Magn. Reson.* 308 (2019) 106600.
- [37] H. Lusic, M.W. Grinstaff, X-ray-computed tomography contrast agents, *Chem. Rev.* 113 (2013) 1641–1666.
- [38] Z. Deng, X. Lin, Z. Huang, J. Meng, Y. Zhong, G. Ma, Y. Zhou, Y. Shen, H. Ding, Y. Huang, Recent progress on advanced imaging techniques for lithium-ion batteries, *Adv. Energy Mater.* 11 (2021) 2000806.
- [39] M. Azevedo, M. Baczyńska, K. Hoffman, A. Krauze, Lithium Mining: How New Production Technologies Could Fuel the Global EV Revolution, McKinsey & Company, 2022.
- [40] A. Breiter, E. Horetsky, M. Linder, R. Rettig, Power Spike: How Battery Makers Can Respond to Surging Demand from EVs, Report, McKinsey & Company, 2022.
- [41] D. Williams, R. Copley, P. Bugryniec, R. Dwyer-Joyce, S. Brown, A review of ultrasonic monitoring: assessing current approaches to Li-ion battery monitoring and their relevance to thermal runaway, *J. Power Sources* 590 (2024) 233777.
- [42] H. Dunegan, D. Harris, Acoustic emission-a new nondestructive testing tool, *Ultrasonics* 7 (1969) 160–166.
- [43] T. Matsuo, M. Uchida, H. Cho, Development of acoustic emission clustering method to detect degradation of lithium ion batteries, *J. Solid Mech. Mater. Eng.* 5 (2011) 678–689.
- [44] S. Komagata, N. Kuwata, R. Baskaran, J. Kawamura, K. Sato, J. Mizusaki, Detection of degradation of lithium-ion batteries with acoustic emission technique, *ECS Trans.* 25 (2010) 163.
- [45] S.-M. Lee, J.-Y. Kim, J. Lee, J.-W. Byeon, Evaluation of cracking damage in electrode materials of a LMO/Al-Lix lithium-ion battery through analysis of acoustic emission signals, *J. Mater. Res. Technol.* 24 (2023) 5235–5249.
- [46] C.-Y. Choe, W.-S. Jung, J.-W. Byeon, Damage evaluation in lithium cobalt oxide/carbon electrodes of secondary battery by acoustic emission monitoring, *Mater. Trans.* 56 (2015) 269–273.
- [47] N. Kircheva, P.-X. Thivel, S. Genies, D. Brun-Buisson, Y. Bultel, Study of SEI formation in Li-ion batteries by acoustic emission technique, *ECS Trans.* 35 (2011) 19.
- [48] S. Didier-Laurent, H. Idrissi, L. Roué, In-situ study of the cracking of metal hydride electrodes by acoustic emission technique, *J. Power Sources* 179 (2008) 412–416.
- [49] A. Tranchot, A. Etienne, P.-X. Thivel, H. Idrissi, L. Roué, In-situ acoustic emission study of Si-based electrodes for Li-ion batteries, *J. Power Sources* 279 (2015) 259–266.
- [50] T. Ohzuku, H. Tomura, K. Sawai, Monitoring of particle fracture by acoustic emission during charge and discharge of Li/MnO₂ cells, *J. Electrochem. Soc.* 144 (1997) 3496.
- [51] Y. Shen, B. Zou, Z. Zhang, M. Xu, S. Wang, Q. Li, H. Li, M. Zhou, K. Jiang, K. Wang, In situ detection of lithium-ion batteries by ultrasonic technologies, *Energy Storage Mater.* 62 (2023) 102915.
- [52] Y. Wu, Y. Wang, W.K. Yung, M. Pecht, Ultrasonic health monitoring of lithium-ion batteries, *Electronics* 8 (2019) 751.
- [53] J.-Y. Kim, J.-H. Jo, J.-W. Byeon, Ultrasonic monitoring performance degradation of lithium ion battery, *Microelectron. Reliab.* 114 (2020) 113859.
- [54] L.P. Bauerma, L.V. Mesquita, C. Bischoff, M. Drews, O. Fitz, A. Heuer, D. Biro, Scanning acoustic microscopy as a non-destructive imaging tool to localize defects inside battery cells, *J. Power Sour. Adv.* 6 (2020) 100035.
- [55] A.G. Hsieh, B.J. Van Tassell, D.A. Steingart, S. Biswas, R.C. Mohr, Arrays of acoustic transducers for physical analysis of batteries, Google Patents (2020).
- [56] J.B. Robinson, R.E. Owen, M.D. Kok, M. Maier, J. Majasan, M. Braglia, R. Stocker, T. Amietzajew, A.J. Roberts, R. Bhagat, Identifying defects in Li-ion cells using ultrasound acoustic measurements, *J. Electrochem. Soc.* 167 (2020) 120530.
- [57] Y.S. Zhang, A.N. Pallipurath Radhakrishnan, J.B. Robinson, R.E. Owen, T. G. Tranter, E. Kendrick, P.R. Shearing, D.J. Brett, In situ ultrasound acoustic measurement of the lithium-ion battery electrode drying process, *ACS Appl. Mater. Interfaces* 13 (2021) 36605–36620.
- [58] M. Yi, F. Jiang, L. Lu, S. Hou, J. Ren, X. Han, L. Huang, Ultrasonic tomography study of metal defect detection in lithium-ion battery, *Front. Energy Res.* 9 (2021) 806929.
- [59] W. Xu, Y. Yang, F. Shi, L. Li, F. Wen, Q. Chen, Ultrasonic phased array imaging of gas evolution in a lithium-ion battery, *Cell Rep. Phys. Sci.* 4 (2023).
- [60] S.J. An, J. Li, Z. Du, C. Daniel, D.L. Wood III, Fast formation cycling for lithium ion batteries, *J. Power Sources* 342 (2017) 846–852.
- [61] D.L. Wood III, J. Li, C. Daniel, Prospects for reducing the processing cost of lithium ion batteries, *J. Power Sources* 275 (2015) 234–242.
- [62] Z. Deng, Z. Huang, Y. Shen, Y. Huang, H. Ding, A. Luscombe, M. Johnson, J. E. Harlow, R. Gauthier, J.R. Dahn, Ultrasonic scanning to observe wetting and “unwetting” in Li-ion pouch cells, *Joule* 4 (2020) 2017–2029.
- [63] S. Hou, M. Yi, F. Jiang, L. Lu, J. Ren, M. Fuhrmann, A. Hascoat, X. Han, X. Lai, Ultrasonic testing-based method for segmental calibration and quantitative estimation of the electrolyte content in lithium-ion batteries, *Measurement* 113101 (2023).
- [64] X. Lai, Y. Huang, C. Deng, H. Gu, X. Han, Y. Zheng, M. Ouyang, Sorting, regrouping, and echelon utilization of the large-scale retired lithium batteries: a critical review, *Renew. Sustain. Energy Rev.* 146 (2021) 111162.
- [65] M. Metzger, B. Strehle, S. Solchenbach, H.A. Gasteiger, Origin of H₂ evolution in LIBs: H₂O reduction vs. electrolyte oxidation, *J. Electrochem. Soc.* 163 (2016) A798.
- [66] R. Fu, S.-Y. Choe, V. Agubra, J. Fergus, Development of a physics-based degradation model for lithium ion polymer batteries considering side reactions, *J. Power Sources* 278 (2015) 506–521.
- [67] R. Fu, S.-Y. Choe, V. Agubra, J. Fergus, Modeling of degradation effects considering side reactions for a pouch type Li-ion polymer battery with carbon anode, *J. Power Sources* 261 (2014) 120–135.
- [68] J. Xu, R.D. Deshpande, J. Pan, Y.-T. Cheng, V.S. Battaglia, Electrode side reactions, capacity loss and mechanical degradation in lithium-ion batteries, *J. Electrochem. Soc.* 162 (2015) A2026.
- [69] A.G. Hsieh, S. Bhadra, B.J. Hertzberg, P.J. Gjeltema, A. Goy, J.W. Fleischer, D. A. Steingart, Electrochemical-acoustic time of flight: in operando correlation of physical dynamics with battery charge and health, *Energ. Environ. Sci.* 8 (2015) 1569–1577.
- [70] G. Davies, K.W. Knehr, B. Van Tassell, T. Hodson, S. Biswas, A.G. Hsieh, D. A. Steingart, State of charge and state of health estimation using electrochemical acoustic time of flight analysis, *J. Electrochem. Soc.* 164 (2017) A2746.
- [71] K. Meng, X. Chen, W. Zhang, W. Chang, J. Xu, A robust ultrasonic characterization methodology for lithium-ion batteries on frequency-domain damping analysis, *J. Power Sources* 547 (2022) 232003.
- [72] P. Ladpli, F. Kopsaftopoulos, F.-K. Chang, Estimating state of charge and health of lithium-ion batteries with guided waves using built-in piezoelectric sensors/actuators, *J. Power Sources* 384 (2018) 342–354.
- [73] H. Huo, K. Huang, W. Luo, J. Meng, L. Zhou, Z. Deng, J. Wen, Y. Dai, Z. Huang, Y. Shen, Evaluating interfacial stability in solid-state pouch cells via ultrasonic imaging, *ACS Energy Lett.* 7 (2022) 650–658.
- [74] C.T. Love, C. Buesser, M.D. Johannes, K.E. Swider-Lyons, Innovating safe lithium-ion batteries through basic to applied research, *J. Electrochem. Energy Convers. Storage* 15 (2018) 011006.
- [75] V. Ruiz, A. Pfarr, A. Kriston, N. Omar, P. Van den Bossche, L. Boon-Brett, A review of international abuse testing standards and regulations for lithium ion batteries in electric and hybrid electric vehicles, *Renew. Sustain. Energy Rev.* 81 (2018) 1427–1452.
- [76] Z. Wang, J. Yuan, X. Zhu, H. Wang, L. Huang, Y. Wang, S. Xu, Overcharge-to-thermal-runaway behavior and safety assessment of commercial lithium-ion cells with different cathode materials: a comparison study, *J. Energy Chem.* 55 (2021) 484–498.
- [77] X. Zhu, H. Wang, X. Wang, Y. Gao, S. Allu, E. Cakmak, Z. Wang, Internal short circuit and failure mechanisms of lithium-ion pouch cells under mechanical indentation abuse conditions: an experimental study, *J. Power Sources* 455 (2020) 227939.
- [78] W. Yuan, D. Liang, Y. Chu, Q. Wang, Aging effect delays overcharge-induced thermal runaway of lithium-ion batteries, *J. Loss Prev. Process Ind.* 79 (2022) 104830.
- [79] J. Arai, Y. Okada, T. Sugiyama, M. Izuka, K. Gotoh, K. Takeda, In situ solid state ⁷Li NMR observations of lithium metal deposition during overcharge in lithium ion batteries, *J. Electrochem. Soc.* 162 (2015) A952.
- [80] D. Lisbona, T. Sne, A review of hazards associated with primary lithium and lithium-ion batteries, *Process Saf. Environ. Prot.* 89 (2011) 434–442.
- [81] D. Juarez-Robles, A.A. Vyas, C. Fear, J.A. Jeevarajan, P.P. Mukherjee, Overdischarge and aging analytics of Li-ion cells, *J. Electrochem. Soc.* 167 (2020) 090558.
- [82] X. Lai, Y. Zheng, L. Zhou, W. Gao, Electrical behavior of overdischarge-induced internal short circuit in lithium-ion cells, *Electrochim. Acta* 278 (2018) 245–254.
- [83] C. Fear, D. Juarez-Robles, J.A. Jeevarajan, P.P. Mukherjee, Elucidating copper dissolution phenomenon in Li-ion cells under overdischarge extremes, *J. Electrochem. Soc.* 165 (2018) A1639.
- [84] C.E. Hendricks, A.N. Mansour, D.A. Fuentevilla, G.H. Waller, J.K. Ko, M.G. Pecht, Copper dissolution in overdischarged lithium-ion cells: X-ray photoelectron spectroscopy and X-ray absorption fine structure analysis, *J. Electrochem. Soc.* 167 (2020) 090501.
- [85] Y. Zheng, K. Qian, D. Luo, Y. Li, Q. Lu, B. Li, Y.-B. He, X. Wang, J. Li, F. Kang, Influence of over-discharge on the lifetime and performance of LiFePO₄/graphite batteries, *RSC Adv.* 6 (2016) 30474–30483.
- [86] Y. Liu, Q. Liu, Z. Li, Y. Ren, J. Xie, H. He, F. Xu, Failure study of commercial LiFePO₄ cells in over-discharge conditions using electrochemical impedance spectroscopy, *J. Electrochem. Soc.* 161 (2014) A620.
- [87] D. Ouyang, J. Weng, M. Chen, J. Wang, Impacts of current rates on the degradation behaviors of lithium-ion batteries under over-discharge conditions, *J. Electrochem. Soc.* 166 (2019) A3432.
- [88] S.-J. Park, Y.-W. Song, B. Kang, M.-J. Kang, M.-Y. Kim, Y.-J. Choi, J. Lim, H. Kim, Y. Hong, Effect of High-temperature thermal management on degradation of li-ion battery for fast charging, *IEEE Trans. Transp. Electrif.* (2023).
- [89] B. Bose, A. Garg, B.K. Panigrahi, J. Kim, Study on Li-ion battery fast charging strategies: review, challenges and proposed charging framework, *J. Storage Mater.* 55 (2022) 105507.
- [90] Z.M. Konz, E.J. McShane, B.D. McCloskey, Detecting the onset of lithium plating and monitoring fast charging performance with voltage relaxation, *ACS Energy Lett.* 5 (2020) 1750–1757.
- [91] C. Fear, T. Adhikary, R. Carter, A.N. Mistry, C.T. Love, P.P. Mukherjee, In operando detection of the onset and mapping of lithium plating regimes during fast charging of lithium-ion batteries, *ACS Appl. Mater. Interfaces* 12 (2020) 30438–30448.

- [92] S.P. Rangarajan, Y. Barsukov, P.P. Mukherjee, Anode potential controlled charging prevents lithium plating, *J. Mater. Chem. A* 8 (2020) 13077–13085.
- [93] S. Xia, L. Mu, Z. Xu, J. Wang, C. Wei, L. Liu, P. Pianetta, K. Zhao, X. Yu, F. Lin, Chemomechanical interplay of layered cathode materials undergoing fast charging in lithium batteries, *Nano Energy* 53 (2018) 753–762.
- [94] P. Yan, J. Zheng, M. Gu, J. Xiao, J.-G. Zhang, C.-M. Wang, Intragranular cracking as a critical barrier for high-voltage usage of layer-structured cathode for lithium-ion batteries, *Nat. Commun.* 8 (2017) 14101.
- [95] Z. Xu, M.M. Rahman, L. Mu, Y. Liu, F. Lin, Chemomechanical behaviors of layered cathode materials in alkali metal ion batteries, *J. Mater. Chem. A* 6 (2018) 21859–21884.
- [96] F. Larsson, B.-E. Mellander, Abuse by external heating, overcharge and short circuiting of commercial lithium-ion battery cells, *J. Electrochem. Soc.* 161 (2014) A1611.
- [97] F. Larsson, P. Andersson, P. Blomqvist, A. Lorén, B.-E. Mellander, Characteristics of lithium-ion batteries during fire tests, *J. Power Sources* 271 (2014) 414–420.
- [98] J.Y. Kim, Z.L. Wang, S.M. Lee, J.W. Byeon, Failure analysis of thermally abused lithium-ion battery cell by microscopy, electrochemical impedance spectroscopy, and acoustic emission, *Microelectron. Reliab.* 100 (2019) 113363.
- [99] H.-P. Lin, D. Chua, M. Salomon, H.C. Shiao, M. Hendrickson, E. Plichta, S. Slane, Low-temperature behavior of Li-ion cells, *Electrochem. Solid St. 4* (2001) A71.
- [100] J. Duan, X. Tang, H. Dai, Y. Yang, W. Wu, X. Wei, Y. Huang, Building safe lithium-ion batteries for electric vehicles: a review, *Electrochem. Energy Rev.* 3 (2020) 1–42.
- [101] Z. Chen, Y. Qin, Y. Ren, W. Lu, C. Orendorff, E.P. Roth, K. Amine, Multi-scale study of thermal stability of lithiated graphite, *Energ. Environ. Sci.* 4 (2011) 4023–4030.
- [102] D.P. Finegan, M. Scheel, J.B. Robinson, B. Tjaden, I. Hunt, T.J. Mason, J. Millichamp, M. Di Michiel, G.J. Offer, G. Hinds, In-operando high-speed tomography of lithium-ion batteries during thermal runaway, *Nat. Commun.* 6 (2015) 6924.
- [103] A.W. Golubkov, D. Fuchs, J. Wagner, H. Wiltsche, C. Stangl, G. Fauler, G. Voitic, A. Thaler, V. Hacker, Thermal-runaway experiments on consumer Li-ion batteries with metal-oxide and olivine-type cathodes, *RSC Adv.* 4 (2014) 3633–3642.
- [104] C.-Y. Wang, G. Zhang, S. Ge, T. Xu, Y. Ji, X.-G. Yang, Y. Leng, Lithium-ion battery structure that self-heats at low temperatures, *Nature* 529 (2016) 515–518.
- [105] M. Qin, Z. Zeng, S. Cheng, J. Xie, Challenges and strategies of formulating low-temperature electrolytes in lithium-ion batteries, *Interdiscipl. Mater.* 2 (2023) 308–336.
- [106] X. Dong, Y. Lin, P. Li, Y. Ma, J. Huang, D. Bin, Y. Wang, Y. Qi, Y. Xia, High-energy rechargeable metallic lithium battery at -70 °C enabled by a cosolvent electrolyte, *Angew. Chem. Int. Ed.* 58 (2019) 5623–5627.
- [107] J. Jaguemont, L. Boulon, Y. Dubé, A comprehensive review of lithium-ion batteries used in hybrid and electric vehicles at cold temperatures, *Appl. Energy* 164 (2016) 99–114.
- [108] C.E.L. Foss, A.M. Svensson, Ø. Gullbrekken, S. Sunde, F. Vullum-Bruer, Temperature effects on performance of graphite anodes in carbonate based electrolytes for lithium ion batteries, *J. Storage Mater.* 17 (2018) 395–402.
- [109] S. Tippmann, D. Walper, L. Balboa, B. Spier, W.G. Bessler, Low-temperature charging of lithium-ion cells part I: Electrochemical modeling and experimental investigation of degradation behavior, *J. Power Sources* 252 (2014) 305–316.
- [110] J. Zhu, Z. Sun, X. Wei, H. Dai, W. Gu, Experimental investigations of an AC pulse heating method for vehicular high power lithium-ion batteries at subzero temperatures, *J. Power Sources* 367 (2017) 145–157.
- [111] H. Li, D. Zhou, M. Zhang, B. Liu, C. Zhang, Multi-field interpretation of internal short circuit and thermal runaway behavior for lithium-ion batteries under mechanical abuse, *Energy* 263 (2023) 126027.
- [112] Z. Zou, F. Xu, H. Tian, X. Niu, Testing and impact modeling of lithium-ion prismatic battery under quasi-static and dynamic mechanical abuse, *J. Storage Mater.* 68 (2023) 107639.
- [113] J. Xu, B. Liu, X. Wang, D. Hu, Computational model of 18650 lithium-ion battery with coupled strain rate and SOC dependencies, *Appl. Energy* 172 (2016) 180–189.
- [114] C. Yuan, L. Wang, S. Yin, J. Xu, Generalized separator failure criteria for internal short circuit of lithium-ion battery, *J. Power Sources* 467 (2020) 228360.
- [115] Y. Jia, B. Liu, Z. Hong, S. Yin, D.P. Finegan, J. Xu, Safety issues of defective lithium-ion batteries: identification and risk evaluation, *J. Mater. Chem. A* 8 (2020) 12472–12484.
- [116] D.P. Finegan, B. Tjaden, T.M. Heenan, R. Jervis, M. Di Michiel, A. Rack, G. Hinds, D.J. Brett, P.R. Shearing, Tracking internal temperature and structural dynamics during nail penetration of lithium-ion cells, *J. Electrochem. Soc.* 164 (2017) A3285.
- [117] B. Liu, Y. Jia, C. Yuan, L. Wang, X. Gao, S. Yin, J. Xu, Safety issues and mechanisms of lithium-ion battery cell upon mechanical abusive loading: a review, *Energy Storage Mater.* 24 (2020) 85–112.
- [118] M. Ohtsu, M. Enoki, Y. Mizutani, M. Shigeishi, M. Ohtsu, Y. Mizutani, M. Ohtsu, M. Ohtsu, M. Ohtsu, M. Shigeishi, Principles of the acoustic emission (AE) method and signal processing, in: *Practical Acoustic Emission Testing*, Springer, 2016, pp. 5–34.
- [119] A. Etienne, H. Idrissi, L. Roué, On the decrepitation mechanism of MgNi and LaNi₅-based electrodes studied by in situ acoustic emission, *J. Power Sources* 196 (2011) 5168–5173.
- [120] R.J. Copley, D. Cumming, Y. Wu, R.S. Dwyer-Joyce, Measurements and modelling of the response of an ultrasonic pulse to a lithium-ion battery as a precursor for state of charge estimation, *J. Storage Mater.* 36 (2021) 102406.
- [121] W. Chang, D. Steingart, Operando 2D acoustic characterization of lithium-ion battery spatial dynamics, *ACS Energy Lett.* 6 (2021) 2960–2968.
- [122] Y. Koyama, T.E. Chin, U. Rhyner, R.K. Holman, S.R. Hall, Y.-M. Chiang, Harnessing the actuation potential of solid-state intercalation compounds, *Adv. Funct. Mater.* 16 (2006) 492–498.
- [123] W. Chang, R. Mohr, A. Kim, A. Raj, G. Davies, K. Denner, J.H. Park, D. Steingart, Measuring effective stiffness of Li-ion batteries via acoustic signal processing, *J. Mater. Chem. A* 8 (2020) 16624–16635.
- [124] Z. Hashin, S. Shtrikman, A variational approach to the theory of the elastic behaviour of multiphase materials, *J. Mech. Phys. Solids* 11 (1963) 127–140.
- [125] M.A. Biot, Theory of elastic waves in a fluid-saturated porous solid. I. Low frequency range, *J. Acoust. Soc. Am.* 28 (1956) 168–178.
- [126] C.M. Atkinson, H.K. Kyötömaa, Acoustic wave speed and attenuation in suspensions, *Int. J. Multiph. Flow* 18 (1992) 577–592.
- [127] M.A. Biot, Theory of propagation of elastic waves in a fluid-saturated porous solid. II. Higher frequency range, *J. Acoust. Soc. Am.* 28 (1956) 179–191.
- [128] J. Achenbach, *Wave Propagation in Elastic Solids*, Elsevier, 2012.
- [129] S.J. Harris, P. Lu, Effects of inhomogeneities nanoscale to mesoscale on the durability of Li-Ion batteries, *J. Phys. Chem. C* 117 (2013) 6481–6492.
- [130] Y. Qi, S.J. Harris, In situ observation of strains during lithiation of a graphite electrode, *J. Electrochem. Soc.* 157 (2010) A741.
- [131] G.E. Backus, Long-wave elastic anisotropy produced by horizontal layering, *J. Geophys. Res.* 67 (1962) 4427–4440.
- [132] K.N. Van Dalen, *Multi-Component Acoustic Characterization of Porous Media*, Springer Science & Business Media, 2013.
- [133] J. Jocker, D. Smets, Ultrasonic measurements on poroelastic slabs: determination of reflection and transmission coefficients and processing for Biot input parameters, *Ultrasonics* 49 (2009) 319–330.
- [134] L. Gold, T. Bach, W. Virsik, A. Schmitt, J. Müller, T.E. Staab, G. Sextl, Probing lithium-ion batteries' state-of-charge using ultrasonic transmission-concept and laboratory testing, *J. Power Sources* 343 (2017) 536–544.
- [135] T.J. Plona, Observation of a second bulk compressional wave in a porous medium at ultrasonic frequencies, *Appl. Phys. Lett.* 36 (1980) 259–261.
- [136] M. Huang, N. Kirkaldy, Y. Zhao, Y. Patel, F. Cegla, B. Lan, Quantitative characterisation of the layered structure within lithium-ion batteries using ultrasonic resonance, *J. Storage Mater.* 50 (2022) 104585.
- [137] C. Martinez-Cisneros, C. Antonelli, B. Levenfeld, A. Varez, J.Y. Sanchez, Evaluation of polyolefin-based macroporous separators for high temperature Li-ion batteries, *Electrochim. Acta* 216 (2016) 68–78.
- [138] M. Ecker, T.K.D. Tran, P. Dechartre, S. Käbitz, A. Warnecke, D.U. Sauer, Parameterization of a physico-chemical model of a lithium-ion battery: I. Determination of parameters, *J. Electrochem. Soc.* 162 (2015) A1836.
- [139] M. Ecker, S. Käbitz, I. Laresgoiti, D.U. Sauer, Parameterization of a physico-chemical model of a lithium-ion battery: II. Model validation, *J. Electrochem. Soc.* 162 (2015) A1849.
- [140] P. Ladpli, F. Kopsaftopoulos, R. Nardari, F.-K. Chang, Battery charge and health state monitoring via ultrasonic guided-wave-based methods using built-in piezoelectric transducers, in: *Smart Materials and Nondestructive Evaluation for Energy Systems 2017*, SPIE, 2017: pp. 53–64.
- [141] Q. Ke, S. Jiang, W. Li, W. Lin, X. Li, H. Huang, Potential of ultrasonic time-of-flight and amplitude as the measurement for state of charge and physical changings of lithium-ion batteries, *J. Power Sources* 549 (2022) 232031.
- [142] E. Gallois, T.G. Tranter, R.E. Owen, J.B. Robinson, P.R. Shearing, D.J. Brett, Battery state-of-charge estimation using machine learning analysis of ultrasonic signatures, *Energy AI* 10 (2022) 100188.
- [143] M. Cieszko, R. Drelich, M. Pakula, Acoustic wave propagation in equivalent fluid macroscopically inhomogeneous materials, *J. Acoust. Soc. Am.* 132 (2012) 2970–2977.
- [144] Z. Yang, H. Yang, T. Tian, D. Deng, M. Hu, J. Ma, D. Gao, J. Zhang, S. Ma, L. Yang, A review in guided-ultrasonic-wave-based structural health monitoring: from fundamental theory to machine learning techniques, *Ultrasonics* (2023).
- [145] H. Kolsky, *Stress Waves in Solids*, Courier Corporation, 1963.
- [146] H. Lamb, On waves in an elastic plate, *Proceedings of the Royal Society of London. Series A, Containing Papers of a Mathematical and Physical Character* 93 (1917) 114–128.
- [147] B.A. Auld, in: *Acoustic Fields and Waves in Solid*, second ed., Krieger Publishing Co, Florida, 1990, pp. 329–330.
- [148] L. Knopoff, A matrix method for elastic wave problems, *Bull. Seismol. Soc. Am.* 54 (1964) 431–438.
- [149] M.J. Randall, Fast programs for layered half-space problems, *Bull. Seismol. Soc. Am.* 57 (1967) 1299–1315.
- [150] G. Jie, Z. Liangheng, L. Yan, S. Fan, W. Bin, H. Cunfu, Ultrasonic guided wave measurement and modeling analysis of the state of charge for lithium-ion battery, *J. Storage Mater.* 72 (2023) 108384.
- [151] G. Song, Y. Li, Y. Lyu, H. Chen, W. Song, J. Gao, C. He, Ultrasonic reflection characteristics of Lithium-ion battery based on Legendre orthogonal polynomial method, *Ultrasonics* 124 (2022) 106736.
- [152] J. Gao, Y. Lyu, C. He, Estimating state of charge of lithium-ion batteries by using ultrasonic guided waves detection technology, *Journal of Physics: Conference Series*, IOP Publishing, 2022.
- [153] N. Kircheva, S. Genies, D. Brun-Buisson, P.-X. Thivel, Study of solid electrolyte interface formation and lithium intercalation in Li-Ion batteries by acoustic emission, *J. Electrochem. Soc.* 159 (2011) A18.
- [154] K. Rhodes, N. Dudney, E. Lara-Curcio, C. Daniel, Understanding the degradation of silicon electrodes for lithium-ion batteries using acoustic emission, *J. Electrochem. Soc.* 157 (2010) A1354.

- [155] Q. Lemarie, F. Alloin, P.-X. Thivel, H. Idrissi, L. Roue, Study of sulfur-based electrodes by operando acoustic emission, *Electrochim. Acta* 299 (2019) 415–422.
- [156] S. Schweidler, S.L. Dreyer, B. Breitung, T. Brezesinski, Operando acoustic emission monitoring of degradation processes in lithium-ion batteries with a high-entropy oxide anode, *Sci. Rep.* 11 (2021) 23381.
- [157] A. Etienne, P. Bernard, H. Idrissi, L. Roué, New insights into the pulverization of LaNi₅-based alloys with different Co contents from electrochemical acoustic emission measurements, *Electrochim. Acta* 186 (2015) 112–116.
- [158] S. Kalnauš, K. Rhodes, C. Daniel, A study of lithium ion intercalation induced fracture of silicon particles used as anode material in Li-ion battery, *J. Power Sources* 196 (2011) 8116–8124.
- [159] A. Gitis, A. Kwade, D.U. Sauer, Flaw detection in the coating process of lithium-ion battery electrodes with acoustic guided waves, *Inst. Stromrichtertech. Elektr. Antriebe ISEA* (2017).
- [160] L. Spithoff, M.S. Wahl, P.J. Vie, O.S. Burheim, Thermal transport in lithium-ion batteries: the effect of degradation, *J. Power Sources* 577 (2023) 233149.
- [161] S. Stock, F. Diller, J. Böhm, L. Hille, J. Hagemeister, A. Sommer, R. Daub, Operando analysis of the gassing and swelling behavior of lithium-ion pouch cells during formation, *J. Electrochem. Soc.* (2023).
- [162] M. Rashid, A. Gupta, Mathematical model for combined effect of SEI formation and gas evolution in Li-ion batteries, *ECS Electrochem. Lett.* 3 (2014) A95.
- [163] N.E. Galushkin, N.N. Yazvinskaya, D.N. Galushkin, Mechanism of gases generation during lithium-ion batteries cycling, *J. Electrochem. Soc.* 166 (2019) A897.
- [164] B. Rowden, N. Garcia-Araez, A review of gas evolution in lithium ion batteries, *Energy Rep.* 6 (2020) 10–18.
- [165] M.T. Pham, J.J. Darst, D.P. Finegan, J.B. Robinson, T.M. Heenan, M.D. Kok, F. Iacoviello, R. Owen, W.Q. Walker, O.V. Magdysyuk, Correlative acoustic time-of-flight spectroscopy and X-ray imaging to investigate gas-induced delamination in lithium-ion pouch cells during thermal runaway, *J. Power Sources* 470 (2020) 228039.
- [166] H. Li, Z. Zhou, Numerical simulation and experimental study of fluid-solid coupling-based air-coupled ultrasonic detection of stomata defect of lithium-ion battery, *Sensors* 19 (2019) 2391.
- [167] M. Fleischhammer, T. Waldmann, G. Bisle, B.-I. Hogg, M. Wohlfahrt-Mehrens, Interaction of cyclic ageing at high-rate and low temperatures and safety in lithium-ion batteries, *J. Power Sources* 274 (2015) 432–439.
- [168] X. Lin, K. Khosravinia, X. Hu, J. Li, W. Lu, Lithium plating mechanism, detection, and mitigation in lithium-ion batteries, *Prog. Energy Combust. Sci.* 87 (2021) 100953.
- [169] X.-G. Yang, Y. Leng, G. Zhang, S. Ge, C.-Y. Wang, Modeling of lithium plating induced aging of lithium-ion batteries: transition from linear to nonlinear aging, *J. Power Sources* 360 (2017) 28–40.
- [170] U.R. Koleti, A. Rajan, C. Tan, S. Moharana, T.Q. Dinh, J. Marco, A study on the influence of lithium plating on battery degradation, *Energies* 13 (2020) 3458.
- [171] T. Ma, D. Xu, M. Wei, H. Wu, X. He, Z. Zhang, D. Ma, S. Liu, B. Fan, C. Lin, Study on lithium plating caused by inconsistent electrode decay rate during aging of traction batteries, *Solid State Ion.* 345 (2020) 115193.
- [172] F.B. Spangler, W. Wittmann, J. Sturm, B. Rieger, A. Jossen, Optimum fast charging of lithium-ion pouch cells based on local volume expansion criteria, *J. Power Sources* 393 (2018) 152–160.
- [173] C. Bommier, W. Chang, Y. Lu, J. Yeung, G. Davies, R. Mohr, M. Williams, D. Steingart, In operando acoustic detection of lithium metal plating in commercial LiCoO₂/graphite pouch cells, *Cell Rep. Phys. Sci.* 1 (2020).
- [174] S.J. An, J. Li, C. Daniel, H.M. Meyer III, S.E. Trask, B.J. Polzin, D.L. Wood III, Electrolyte volume effects on electrochemical performance and solid electrolyte interphase in Si-graphite/NMC lithium-ion pouch cells, *ACS Appl. Mater. Interfaces* 9 (2017) 18799–18808.
- [175] C. Zhao, Z. Yang, X. Zhou, Z. Hao, J. Chen, Z. Wang, X. Chen, X. Wu, L. Li, L. Li, Recent progress on electrolyte boosting initial coulombic efficiency in lithium-ion batteries, *Adv. Funct. Mater.* (2023).
- [176] J. Henschel, F. Horsthemke, Y.P. Stenzel, M. Evertz, S. Girod, C. Lürenbaum, K. Kösters, S. Wiemers-Meyer, M. Winter, S. Nowak, Lithium ion battery electrolyte degradation of field-tested electric vehicle battery cells—a comprehensive analytical study, *J. Power Sources* 447 (2020) 227370.
- [177] F. Lv, Z. Wang, L. Shi, J. Zhu, K. Edström, J. Mindemark, S. Yuan, Challenges and development of composite solid-state electrolytes for high-performance lithium ion batteries, *J. Power Sources* 441 (2019) 227175.
- [178] X. Han, L. Lu, Y. Zheng, X. Feng, Z. Li, J. Li, M. Ouyang, A review on the key issues of the lithium ion battery degradation among the whole life cycle, *Etransportation* 1 (2019) 100005.
- [179] X. Wang, X. Wei, J. Zhu, H. Dai, Y. Zheng, X. Xu, Q. Chen, A review of modeling, acquisition, and application of lithium-ion battery impedance for onboard battery management, *Etransportation* 7 (2021) 100093.
- [180] B. Salomez, S. Grignon, M. Armand, P. Tran-Van, S. Laruelle, Gassing mechanisms in lithium-ion battery, *J. Electrochem. Soc.* 170 (2023) 050537.
- [181] M.C. Appleberry, J.A. Kowalski, S.A. Africk, J. Mitchell, T.C. Ferree, V. Chang, V. Parekh, Z. Xu, Z. Ye, J.F. Whitacre, Avoiding thermal runaway in lithium-ion batteries using ultrasound detection of early failure mechanisms, *J. Power Sources* 535 (2022) 231423.
- [182] C. Bommier, W. Chang, J. Li, S. Biswas, G. Davies, J. Nanda, D. Steingart, Operando acoustic monitoring of SEI formation and long-term cycling in NMC/SiGr composite pouch cells, *J. Electrochem. Soc.* 167 (2020) 020517.
- [183] H. Sun, N. Muralidharan, R. Amin, V. Rathod, P. Ramuhalli, I. Belharouak, Ultrasonic nondestructive diagnosis of lithium-ion batteries with multiple frequencies, *J. Power Sources* 549 (2022) 232091.
- [184] X. Wu, X. Li, J. Du, State of charge estimation of lithium-ion batteries over wide temperature range using unscented Kalman filter, *IEEE Access* 6 (2018) 41993–42003.
- [185] W.-Y. Chang, The state of charge estimating methods for battery: a review, *Int. Schol. Res. Notices* 2013 (2013).
- [186] M.A. Hannan, M.H. Lipu, A. Hussain, A. Mohamed, A review of lithium-ion battery state of charge estimation and management system in electric vehicle applications: challenges and recommendations, *Renew. Sustain. Energy Rev.* 78 (2017) 834–854.
- [187] D.N. How, M.A. Hannan, M.H. Lipu, P.J. Ker, State of charge estimation for lithium-ion batteries using model-based and data-driven methods: a review, *IEEE Access* 7 (2019) 136116–136136.
- [188] N. Yang, X. Zhang, B. Shang, G. Li, Unbalanced discharging and aging due to temperature differences among the cells in a lithium-ion battery pack with parallel combination, *J. Power Sources* 306 (2016) 733–741.
- [189] R. Xiong, J. Cao, Q. Yu, H. He, F. Sun, Critical review on the battery state of charge estimation methods for electric vehicles, *IEEE Access* 6 (2017) 1832–1843.
- [190] S. Lee, J. Kim, J. Lee, B.H. Cho, State-of-charge and capacity estimation of lithium-ion battery using a new open-circuit voltage versus state-of-charge, *J. Power Sources* 185 (2008) 1367–1373.
- [191] S. Rodrigues, N. Munichandraiah, A.K. Shukla, AC impedance and state-of-charge analysis of a sealed lithium-ion rechargeable battery, *J. Solid State Electrochem.* 3 (1999) 397–405.
- [192] J. Xu, C.C. Mi, B. Cao, J. Cao, A new method to estimate the state of charge of lithium-ion batteries based on the battery impedance model, *J. Power Sources* 233 (2013) 277–284.
- [193] K.S. Ng, C.-S. Moo, Y.-P. Chen, Y.-C. Hsieh, Enhanced coulomb counting method for estimating state-of-charge and state-of-health of lithium-ion batteries, *Appl. Energy* 86 (2009) 1506–1511.
- [194] X. Han, M. Ouyang, L. Lu, J. Li, Simplification of physics-based electrochemical model for lithium ion battery on electric vehicle. Part II: Pseudo-two-dimensional model simplification and state of charge estimation, *J. Power Sources* 278 (2015) 814–825.
- [195] S.J. Moura, N.A. Chaturvedi, M. Krstic, PDE estimation techniques for advanced battery management systems—Part I: SOC estimation, in: 2012 American Control Conference (ACC), IEEE, 2012, pp. 559–565.
- [196] M. Corno, N. Bhatt, S.M. Savarese, M. Verhaegen, Electrochemical model-based state of charge estimation for Li-ion cells, *IEEE Trans. Control Syst. Technol.* 23 (2014) 117–127.
- [197] C. Lin, A. Tang, J. Xing, Evaluation of electrochemical models based battery state-of-charge estimation approaches for electric vehicles, *Appl. Energy* 207 (2017) 394–404.
- [198] U. Westerhoff, T. Kroker, K. Kurbach, M. Kurat, Electrochemical impedance spectroscopy based estimation of the state of charge of lithium-ion batteries, *J. Storage Mater.* 8 (2016) 244–256.
- [199] W. Waag, S. Käbitz, D.U. Sauer, Experimental investigation of the lithium-ion battery impedance characteristic at various conditions and aging states and its influence on the application, *Appl. Energy* 102 (2013) 885–897.
- [200] S. Tong, J.H. Lacap, J.W. Park, Battery state of charge estimation using a load-classifying neural network, *J. Storage Mater.* 7 (2016) 236–243.
- [201] D. Cui, B. Xia, R. Zhang, Z. Sun, Z. Lao, W. Wang, W. Sun, Y. Lai, M. Wang, A novel intelligent method for the state of charge estimation of lithium-ion batteries using a discrete wavelet transform-based wavelet neural network, *Energies* 11 (2018) 995.
- [202] F. Yang, X. Song, F. Xu, K.-L. Tsui, State-of-charge estimation of lithium-ion batteries via long short-term memory network, *IEEE Access* 7 (2019) 53792–53799.
- [203] T. Hansen, C.-J. Wang, Support vector based battery state of charge estimator, *J. Power Sources* 141 (2005) 351–358.
- [204] V. Klass, M. Behm, G. Lindbergh, A support vector machine-based state-of-health estimation method for lithium-ion batteries under electric vehicle operation, *J. Power Sources* 270 (2014) 262–272.
- [205] A.J. Salkind, C. Fennie, P. Singh, T. Atwater, D.E. Reisner, Determination of state-of-charge and state-of-health of batteries by fuzzy logic methodology, *J. Power Sources* 80 (1999) 293–300.
- [206] P. Singh, R. Vinjamuri, X. Wang, D. Reisner, Design and implementation of a fuzzy logic-based state-of-charge meter for Li-ion batteries used in portable defibrillators, *J. Power Sources* 162 (2006) 829–836.
- [207] Z. Chen, X. Li, J. Shen, W. Yan, R. Xiao, A novel state of charge estimation algorithm for lithium-ion battery packs of electric vehicles, *Energies* 9 (2016) 710.
- [208] J. Xu, B. Cao, Z. Chen, Z. Zou, An online state of charge estimation method with reduced prior battery testing information, *Int. J. Electr. Power Energy Syst.* 63 (2014) 178–184.
- [209] J.H. Lee, H.M. Lee, S. Ahn, Battery dimensional changes occurring during charge/discharge cycles—thin rectangular lithium ion and polymer cells, *J. Power Sources* 119 (2003) 833–837.
- [210] X. Wang, Y. Sone, S. Kuwajima, In situ investigation of the volume change in Li-ion cell with charging and discharging: Satellite power applications, *J. Electrochem. Soc.* 151 (2004) A273.
- [211] D. Ensminger, L.J. Bond, *Ultrasonics: Fundamentals, Technologies, and Applications*, CRC Press, 2011.

- [212] P. Albertus, J. Newman, Introduction to dualfoil 5.0, University of California Berkeley, Berkeley, CA, 2007. Tech. Rep.
- [213] J.N. Reimers, J.R. Dahn, Electrochemical and in situ X-ray diffraction studies of lithium intercalation in Li_xCoO₂, *J. Electrochem. Soc.* 139 (1992) 2091.
- [214] Y. Qi, H. Guo, L.G. Hector, A. Timmons, Threefold increase in the Young's modulus of graphite negative electrode during lithium intercalation, *J. Electrochem. Soc.* 157 (2010) A558.
- [215] L. Wu, J. Zhang, Ab initio study of anisotropic mechanical properties of LiCoO₂ during lithium intercalation and deintercalation process, *J. Appl. Phys.* 118 (2015).
- [216] J.-J. Chang, X.-F. Zeng, T.-L. Wan, Real-time measurement of lithium-ion batteries' state-of-charge based on air-coupled ultrasound, *AIP Adv.* 9 (2019).
- [217] J.B. Robinson, M. Pham, M.D. Kok, T.M. Heenan, D.J. Brett, P.R. Shearing, Examining the cycling behaviour of Li-ion batteries using ultrasonic time-of-flight measurements, *J. Power Sources* 444 (2019) 227318.
- [218] Z. Cai, T. Pan, H. Jiang, Z. Li, Y. Wang, State-of-charge estimation of lithium-ion batteries based on ultrasonic detection, *J. Storage Mater.* 65 (2023) 107264.
- [219] Y. Wei, Y. Yan, C. Zhang, K. Meng, C. Xu, State estimation of lithium-ion batteries based on the initial rise time feature of ultrasonic signals, *J. Power Sources* 581 (2023) 233497.
- [220] Z. Huang, Y. Zhou, Z. Deng, K. Huang, M. Xu, Y. Shen, Y. Huang, Precise state-of-charge mapping via deep learning on ultrasonic transmission signals for lithium-ion batteries, *ACS Appl. Mater. Interfaces* 15 (2023) 8217–8223.
- [221] X. Li, C. Wu, C. Fu, S. Zheng, J. Tian, State characterization of lithium-ion battery based on ultrasonic guided wave scanning, *Energies* 15 (2022) 6027.
- [222] P. Ladpli, C. Liu, F. Kopsaftopoulos, F.-K. Chang, Estimating lithium-ion battery state of charge and health with ultrasonic guided waves using an efficient matching pursuit technique, in: IEEE Transportation Electrification Conference and Expo, Asia-Pacific (ITEC Asia-Pacific), IEEE, 2018, pp. 1–5.
- [223] S.G. Mallat, Z. Zhang, Matching pursuits with time-frequency dictionaries, *IEEE Trans. Signal Process.* 41 (1993) 3397–3415.
- [224] H. Popp, M. Koller, S. Keller, G. Glanz, R. Klambauer, A. Bergmann, State estimation approach of lithium-ion batteries by simplified ultrasonic time-of-flight measurement, *IEEE Access* 7 (2019) 170992–171000.
- [225] G. Zhao, Y. Liu, G. Liu, S. Jiang, W. Hao, State-of-charge and state-of-health estimation for lithium-ion battery using the direct wave signals of guided wave, *J. Storage Mater.* 39 (2021) 102657.
- [226] Y. Liu, R. Zhang, W. Hao, Evaluation of the state of charge of lithium-ion batteries using ultrasonic guided waves and artificial neural network, *Ionics* 28 (2022) 3277–3288.
- [227] X. Li, W. Hua, C. Wu, S. Zheng, Y. Tian, J. Tian, State estimation of a lithium-ion battery based on multi-feature indicators of ultrasonic guided waves, *J. Storage Mater.* 56 (2022) 106113.
- [228] S. Yang, C. Zhang, J. Jiang, W. Zhang, L. Zhang, Y. Wang, Review on state-of-health of lithium-ion batteries: characterizations, estimations and applications, *J. Clean. Prod.* 314 (2021) 128015.
- [229] M. Dubarry, G. Baure, D. Anseán, Perspective on state-of-health determination in lithium-ion batteries, *J. Electrochem. Energy Convers. Storage* 17 (2020) 044701.
- [230] X. Zhou, J.L. Stein, T. Ersal, Battery state of health monitoring by estimation of the number of cyclable Li-ions, *Control Eng. Pract.* 66 (2017) 51–63.
- [231] G.K. Prasad, C.D. Rahn, Model based identification of aging parameters in lithium ion batteries, *J. Power Sources* 232 (2013) 79–85.
- [232] T. Kim, Y. Wang, Z. Sahinoglu, T. Wada, S. Hara, W. Qiao, Fast UD factorization-based RLS online parameter identification for model-based condition monitoring of lithium-ion batteries, in: 2014 American Control Conference, IEEE, 2014, pp. 4410–4415.
- [233] P. Singh, C. Chen, C.M. Tan, S.-C. Huang, Semi-Empirical capacity fading model for SoH estimation of Li-Ion batteries, *Appl. Sci.* 9 (2019) 3012.
- [234] Y. Li, K. Liu, A.M. Foley, A. Zülke, M. Berecibar, E. Nanini-Maury, J. Van Mierlo, H.E. Hoster, Data-driven health estimation and lifetime prediction of lithium-ion batteries: a review, *Renew. Sustain. Energy Rev.* 113 (2019) 109254.
- [235] Y. Wu, W. Li, Y. Wang, K. Zhang, Remaining useful life prediction of lithium-ion batteries using neural network and bat-based particle filter, *IEEE Access* 7 (2019) 54843–54854.
- [236] D. Liu, Y. Luo, J. Liu, Y. Peng, L. Guo, M. Pecht, Lithium-ion battery remaining useful life estimation based on fusion nonlinear degradation AR model and RPF algorithm, *Neural Comput. Appl.* 25 (2014) 557–572.
- [237] H. Tian, P. Qin, K. Li, Z. Zhao, A review of the state of health for lithium-ion batteries: research status and suggestions, *J. Clean. Prod.* 261 (2020) 120813.
- [238] B. Sood, M. Osterman, M. Pecht, Health monitoring of lithium-ion batteries, in: IEEE Symposium on Product Compliance Engineering (ISPCE), IEEE, 2013, pp. 1–6.
- [239] K.W. Knehr, T. Hodson, C. Bommier, G. Davies, A. Kim, D.A. Steingart, Understanding full-cell evolution and non-chemical electrode crosstalk of Li-ion batteries, *Joule* 2 (2018) 1146–1159.